January 2022

Development Of A Piezo-Mechanical Battery

Caleb Aba-Onukaogu Aba-Onukaogu

DEVELOPMENT OF A PIEZO-MECHANICAL BATTERY

by

Caleb Chukwuemeka Aba-Onukaogu

Bachelor of Science, Covenant University, 2018

A Thesis

Submitted to the Graduate Faculty

of the

University of North Dakota

in partial fulfillment of the requirement

for the degree of

Master of Science

Grand Forks, North Dakota

May

2022

This thesis submitted by Caleb Chukwuemeka Aba-Onukaogu in partial fulfillment of the requirements for the Degree of Master of Science from the University of North Dakota, has been read by the Faculty Advisory Committee under whom the work has been done and hereby approved.

_____

Dr. Djedje-Kossu Zahui

_____

Date

_____

Dr. Roy Sougata

_____

Date

_____

Dr. Hallie Chelmo

_____

Date

The appointed advisory committee is submitting this thesis as having met all the requirements of the School of Graduate Studies at the University of North Dakota and is hereby approved.

_____

Chris Nelson

Dean of the School of Graduate Studies

_____

Date

PERMISSION

Title   DEVELOPMENT OF A PIEZO-MECHANICAL BATTERY

Department   Mechanical Engineering

Degree   Master of Science

In presenting this thesis in partial fulfillment of the requirements for a graduate degree from the University of North Dakota, I agree that the library of the University shall make it freely available for inspection. I further agree that the permission for extensive copying for scholarly purposes may be granted by the professor who supervised my thesis work or, in his absence, by the Chairperson of the department or the dean of the School of Graduate Studies. It is understood that any copying or publication or other use of this thesis or part thereof for financial gain shall not be allowed without my written permission. It is also understood that due recognition shall be given to me and to the University of North Dakota in any scholarly use which may be made of any material in my thesis.

<div align="right">

Caleb C. Aba-Onukaogu

May 2022

</div>

TABLE OF CONTENTS

TABLE OF FIGURES

LIST OF TABLES

ACKNOWLEDGEMENT

This project could not have been completed without the help of many people. I would like to start with the University of North Dakota Mechanical Engineering Department for providing me the opportunity to continue my education in their graduate program. I would also like to thank Dr. Zahui for advising me throughout the duration of the project and for the guidance he provided me over the two years I worked under him. This help over the years is appreciated. I have to thank my advisory committee members, Dr. Roy Sougata and Dr. Hallie Chelmo for their support. I would like to express my gratitude to every faculty and staff of UND that has been of help throughout my stay here.

I would like to acknowledge my family and friends for being a strong support and cheering me all the way. God bless you!

ABSTRACT

The piezo-mechanical battery is designed to store energy in a flat spiral spring and harvest the kinetic energy of the unwinding spring using piezoelectric unimorph cantilever beams. The system, initially proposed on a micro scale, was designed to function on a macro scale. The power spring of the system was designed to deliver enough torque to run the system and provide enough force to the escapement mechanism to excite the cantilever beams. The gear system is designed as a compound epicyclic gear system with a gear ratio of 55:1. The cantilever beams were designed to act as springs as well as harvesters in the system. The runtime of the system was estimated to be 220 seconds. The proposed design was tested numerically as well as experimentally to prove that the system integration works. Experiments to prove the power output from a piezoelectric cantilever beam were also carried out.

The maximum torque delivered by the spring is 0.08Nm and the dimensions of the escapement mechanism translates the output torque to 0.37N of force on the cantilever beams. The final assembly of the device is 4 inches tall and 7 inches across and so the objective of portability was somewhat achieved.

CHAPTER 1
1   INTRODUCTION

1.1   Overview

Over the last two centuries, the human race has seen a lot of advancement in technology that has improved our way of life. As a result of this, the demand for energy and power has also greatly increased. Earlier technologies made use of wood , charcoal, and other biofuels to generate power but with time, they would not be able to keep up. Enter electricity. From the early 19th century, we have become more reliant on electricity to go about our daily lives to the point where electricity is indispensable to the society. From powering our homes and powering the second industrial revolution to powering our mobile devices and automobiles nowadays. (George, 2019). Changes in levels of energy consumption, both for individual countries and for the world as a whole, are in a symbiotic relationship with levels of both population and wealth. That is, increasing access to energy makes it possible for human society to support larger populations and increasing levels of wealth, while at the same time, a growing population and increasing wealth will spur the purchase of energy for all aspects of daily life. In our effort to generate electricity to meet the demands of the population, we have tried many sources such as fossil fuels, coal and natural gas which have been the major sources for some time now as seen in Figure 1.1 (BP Statistical review of world energy, 2018). Energy generation has come at a cost to the earth. Studies have shown a direct correlation between the burning of fossil fuels and climate change. In recent years, the world is more aware of the impact that greenhouse gases have on the environment. This has led to an increased demand for eco-friendly renewable energy. Although environmentally friendly sources such as hydroelectric, solar

and wind are available and being adopted in various scales worldwide; governmental policies, infrastructural challenges, geographical and economic factors often impede mass adoption of such renewable energy sources (George, 2019).

Shares of global primary energy consumption by fuel
Percentage
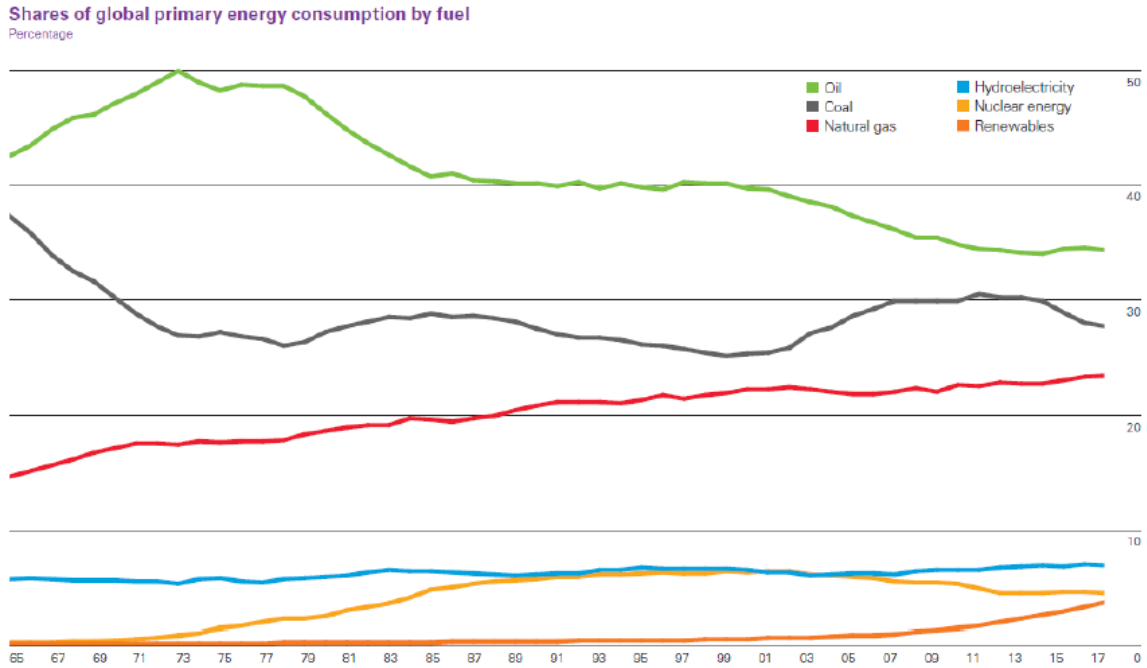
Figure 1-1 Global usage of energy sources including fossil fuels and renewables (BP Statistical Review of World Energy, 2018)

The rapid advancement of technology has brought about smart, portable electronic devices and in response to the increasing requirements of these systems for energy, demand has also increased for more efficient and higher density energy storage systems that are eco-friendly. The storage systems are essential to providing power for small systems like micro-electromechanical systems (MEMs), portable electronics or for storing energy from intermittent renewable power sources like wind or solar which sometimes see an excess of energy followed by a period of low or no energy generated. Batteries, supercapacitors, compressed gas, pumped hydro mechanical springs and flywheels are all currently used to

2

store excess energy generated. Batteries are most commonly used but they have drawbacks like their low energy density, long recharge times, limited operating temperature range and low power densities. Mechanical energy storage devices, even with energy densities typically lower than batteries, have the ability to deliver energy in a reliable and environmentally safe way while also being suited for most modes of usage.

Piezoelectric materials are eco-friendly, renewable energy generation materials which are widely used in electro-mechanical systems. Some applications use the converse piezoelectric effect but by making use of the direct piezoelectric effect, we can be able to generate electricity from mechanically stored energy. This is achieved by exciting flexible piezoelectric materials e.g., Polyvinylidene fluoride (PVDF) while it is connected to an energy harvester system. Piezoelectric generators have a small number of moving parts, an energy conversion efficiency as high as 80% (C. D. Richards, 2004).

The study made in this research focuses on the development of a Piezo-Mechanical-Battery (PMB) by applying the direct piezoelectric effect. The material of choice is PVDF. PVDF is widely used in energy harvesters. This research uses experimental approach as well as analytical techniques to develop and optimize the battery.

1.2   Piezoelectric Materials

The ability of a material to give out electrical charge under mechanical deformation is known as piezoelectricity. The term "piezo" derives from the Greek meaning "to press" (R. S. Dahiya, 2013). The phenomenon was discovered by the Curie brothers in 1880 who found that materials like topaz and quartz were accompanied by macroscopic polarization which produces the electric surface charges (D., 1995). Piezoelectric materials are a class of dielectric materials which can be polarized by an electric field and a mechanical stress

3

which is called the piezoelectric effect. The piezoelectric effect is a phenomenon by which certain dielectric materials (with non-center symmetries, excluding the 432 point group) generate an electric charge in response to applied mechanical stress (direct piezoelectric effect), or generate mechanical strain/displacement under an applied electric field (converse piezoelectric effect) (S. Trolier-McKinstry, 2018). Piezoelectric materials consist of polymers and ceramics. A large number of piezoelectric ceramics are of the perovskite family which are made of mixed oxides of oxygen ions which include lithium niobate ($LiNbO_3$), lithium tantalite ($LiTaO_3$), barium titanate ($BaTiO_3$), lead titanate ($PbTiO_3$) (Freitas, 2011). The most common ceramic piezoelectric material is the PZT which is a binary solution of lead zirconate (PZ, an antiferroelectric) and lead titanate (PT, a ferroelectric) that is often doped with niobium or lanthanum to form soft and hard piezoelectric materials, respectively.

Quartz (SiO_2) is a ceramic that was first commercial exploited as a piezoelectric material. It has high permissible surface pressure of about 150 N/mm^2, can withstand temperatures up to 500 ^{O}C, very high rigidity, high linearity and negligible hysteresis, constant sensitivity over a wide temperature range which all make Quartz an excellent piezoelectric material.

Zinc Oxide is a relatively soft piezoelectric material which has been used in MEMs as surface wave (WAS) or bulk acoustic wave (BAW) resonators. The pressure-sensing ability was investigated by Kuoni et al (A. Kuoni, 2003). They studied the ZnO thin film that were placed in various positions of flow chamber to measure the liquid pressure difference, thus indicating the flow speed.

PVDF is a polymer that has become appealing to many industries due to its striking characteristics. They are inexpensive, lightweight, biologically compatible, mechanically stable structures and have high electromechanical coefficients which make them suitable as a piezoelectric sensor. They can undergo significant amount of deformation under mechanical stress.

PVDF and PZT both have their advantages and disadvantages. To optimize the performance of a piezoelectric material, the combined properties of ceramic and polymer is considered. Composites are multiphase materials which show the properties of both ceramic and polymers. They are composed of two phases: Matrix phase and dispersed or discrete phase. Dispersed phase refers to the distribution of particles of one constituent and matrix phase surrounds the dispersed phase to make a continuous medium (Bolaniran, 2021).

1.3   The Piezoelectric Effect

The piezoelectric effect is the generation of an electric charge in response to a force exerted on the material.
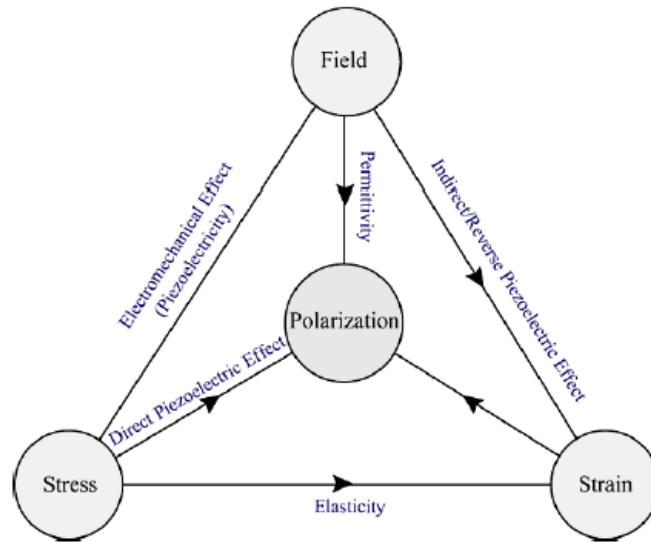
Figure 1-2 Piezoelectricity—An intermingling of electric and elastic phenomena (Dahiya, 2013)

The centers of the negative and positive charges of each molecule correspond before the material is subjected to external forces. This means the molecule is electrically neutral as seen in Figure 1.3(a). The internal reticular is deformed in the presence of an external mechanical stress, thus causing the separation of the positive and negative centers of the molecule, and generating little dipoles as seen in Figure 1.3(b). This results in the opposite facing poles inside the material canceling each other and fixed charges appear on the surface. This is shown in Figure 1.3(c). What this means is that the material is polarized, and the effect is called the direct piezoelectric effect. This polarization generates an electric field that can be used to transform the mechanical energy, used in the material's deformation, into electrical energy. (R. S. Dahiya, 2013)
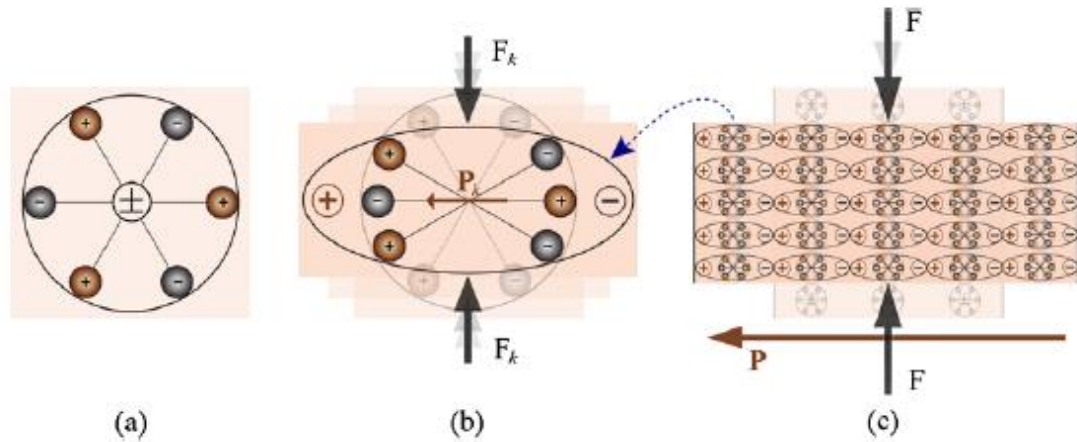
Figure 1-3 Piezoelectric effect explained with a simple molecular model (R. S. Dahiya, 2013)

1.4   Piezoelectric Effect — Basic Mathematical Formulation

As previously explained, when a pole piezoelectric material is mechanically strained, it becomes electrically polarized and produces a fixed electric charge on the surface. Following the linear theory of piezoelectricity (J. Wu, 1996), the density of generated fixed charge in a piezoelectric material is proportional to the external stress. It can be formulated as

$$P_{pe} = d \times T \qquad (1\text{-}1)$$

Where P_{pe} is the piezoelectric polarization vector and the magnitude is equal to the fixed chare density produced as a result of piezoelectric effect., d is the piezoelectric strain coefficient and T is the stress on the piezoelectric material. For simplicity, the polarization, stress, and the strain generated by the piezoelectric effect have been specified with the '*pe*' subscript, while those externally applied do not have any subscript.

Similarly, the indirect/reverse piezoelectric effect can be written as

7

$$S_{pe} = d \times E \qquad\qquad (1\text{-}2)$$

Where S_{pe} is the mathematical strain produced by the reverse piezoelectric effect and E is the magnitude of the applied electric field. Considering the elastic properties of the material, the direct and reverse piezoelectric effects can alternatively be formulated as:

$$P_{pe} = d \times T = d \times c \times S = e \times S \qquad\qquad (1\text{-}3)$$

$$T_{pe} = c \times S_{pe} = c \times d \times E = e \times E \qquad\qquad (1\text{-}4)$$

Where c is the elastic constant relating the generated stress and the applied strain ($T = c \times S$), s is the compliance coefficient which relates the deformation produced by the application of a stress ($S = s \times T$), and e is the piezoelectric stress constant.

The piezoelectricity is a cross coupling between the elastic variables, stress T and Strain S, and the dielectric variables, electric charge density D and electric field E. The tensor relation to identify this coupling is given as:

$$S_p = s_{pq}^E T_q + d_{pk} E_k \qquad\qquad (1\text{-}5)$$

$$D_i = d_{iq} T_q + \varepsilon_{ik}^T E_k \qquad\qquad (1\text{-}6)$$

where s_{pg}^E is elastic compliance tensor at constant electric field, ε_{ik}^T is dielectric constant tensor under constant stress, d_{kp} is piezoelectric constant tensor, S_p is the mechanical strain in p direction, D_i is electric displacement in i direction, T_q is mechanical stress in q direction, and E_k is the electric field in the k direction (R. S. Dahiya, 2013).

1.5   Piezoelectric Linear Constitutive Relations

As the tensor direction illustrated in Fig. 1.4 for piezoelectric materials such as PVDF, the stretch direction is denoted as "1" and the axis orthogonal to the stretch direction in the plane of the film becomes "2". The polarization axis (perpendicular to the surface of the film) is denoted as "3".

Figure 1-4 Tensor directions for defining the constitutive relations

The shear planes are indicated by the subscripts "4", "5", "6" and are perpendicular to the directions "1", "2" and "3" respectively. Applying this directions, Eqn. (1-5) and (1-6) can be written as:

$$
\begin{bmatrix} S_1 \\ S_2 \\ S_3 \\ S_4 \\ S_5 \\ S_6 \end{bmatrix} =
\begin{bmatrix}
s_{11}^E & s_{12}^E & s_{13}^E & s_{14}^E & s_{15}^E & s_{16}^E \\
s_{21}^E & s_{22}^E & s_{23}^E & s_{24}^E & s_{25}^E & s_{26}^E \\
s_{31}^E & s_{32}^E & s_{33}^E & s_{34}^E & s_{35}^E & s_{36}^E \\
s_{41}^E & s_{42}^E & s_{43}^E & s_{44}^E & s_{45}^E & s_{46}^E \\
s_{51}^E & s_{52}^E & s_{53}^E & s_{54}^E & s_{55}^E & s_{56}^E \\
s_{61}^E & s_{62}^E & s_{63}^E & s_{64}^E & s_{65}^E & s_{66}^E
\end{bmatrix}
\begin{bmatrix} T_1 \\ T_2 \\ T_3 \\ T_4 \\ T_5 \\ T_6 \end{bmatrix} +
\begin{bmatrix}
d_{11} & d_{12} & d_{13} \\
d_{21} & d_{22} & d_{23} \\
d_{31} & d_{32} & d_{33} \\
d_{41} & d_{42} & d_{43} \\
d_{51} & d_{52} & d_{53} \\
d_{61} & d_{62} & d_{63}
\end{bmatrix}
\begin{bmatrix} E_1 \\ E_2 \\ E_3 \end{bmatrix}
\qquad (1\text{-}7)
$$

$$
\begin{bmatrix} D_1 \\ D_2 \\ D_3 \end{bmatrix} =
\begin{bmatrix}
d_{11} & d_{12} & d_{13} & d_{14} & d_{15} & d_{16} \\
d_{21} & d_{22} & d_{23} & d_{24} & d_{25} & d_{26} \\
d_{31} & d_{32} & d_{33} & d_{34} & d_{35} & d_{36}
\end{bmatrix}
\begin{bmatrix} T_1 \\ T_2 \\ T_3 \\ T_4 \\ T_5 \\ T_6 \end{bmatrix} +
\begin{bmatrix}
\varepsilon_{11}^T & \varepsilon_{12}^T & \varepsilon_{13}^T \\
\varepsilon_{12}^T & \varepsilon_{22}^T & \varepsilon_{23}^T \\
\varepsilon_{31}^T & \varepsilon_{32}^T & \varepsilon_{33}^T
\end{bmatrix}
\begin{bmatrix} E_1 \\ E_2 \\ E_3 \end{bmatrix}
\qquad (1\text{-}8)
$$

It is observed that the piezoelectric coefficients, d_{ij} for the mechanical and the electrical responses are identical giving opportunity to develop the global response by a matrix that couple both the electrical and mechanical behaviors as written here

$$
\begin{Bmatrix} S_1 \\ S_2 \\ S_3 \\ S_4 \\ S_5 \\ S_6 \\ D_1 \\ D_2 \\ D_3 \end{Bmatrix} =
\begin{bmatrix}
S_{11}^{ET} & S_{12}^{ET} & S_{13}^{ET} & S_{14}^{ET} & S_{15}^{ET} & S_{16}^{ET} & d_{11}^{T\theta} & d_{12}^{T\theta} & d_{13}^{T\theta} \\
S_{21}^{ET} & S_{22}^{ET} & S_{23}^{ET} & S_{24}^{ET} & S_{25}^{ET} & S_{26}^{ET} & d_{22}^{T\theta} & d_{22}^{T\theta} & d_{23}^{T\theta} \\
S_{31}^{ET} & S_{32}^{ET} & S_{33}^{ET} & S_{34}^{ET} & S_{35}^{ET} & S_{36}^{ET} & d_{31}^{T\theta} & d_{32}^{T\theta} & d_{33}^{T\theta} \\
S_{41}^{ET} & S_{42}^{ET} & S_{43}^{ET} & S_{44}^{ET} & S_{45}^{ET} & S_{46}^{ET} & d_{41}^{T\theta} & d_{42}^{T\theta} & d_{43}^{T\theta} \\
S_{51}^{ET} & S_{52}^{ET} & S_{53}^{ET} & S_{54}^{ET} & S_{55}^{ET} & S_{56}^{ET} & d_{51}^{T\theta} & d_{52}^{T\theta} & d_{53}^{T\theta} \\
S_{61}^{ET} & S_{62}^{ET} & S_{63}^{ET} & S_{64}^{ET} & S_{65}^{ET} & S_{66}^{ET} & d_{61}^{T\theta} & d_{62}^{T\theta} & d_{63}^{T\theta} \\
d_{11}^{E.T} & d_{12}^{E.T} & d_{13}^{E.T} & d_{14}^{E.T} & d_{15}^{E.T} & d_{16}^{E.T} & \varepsilon_{11}^T & \varepsilon_{12}^T & \varepsilon_{13}^T \\
d_{21}^{E.T} & d_{22}^{E.T} & d_{23}^{E.T} & d_{24}^{E.T} & d_{25}^{E.T} & d_{26}^{E.T} & \varepsilon_{12}^T & \varepsilon_{22}^T & \varepsilon_{23}^T \\
d_{31}^{E.T} & d_{32}^{E.T} & d_{33}^{E.T} & d_{34}^{E.T} & d_{35}^{E.T} & d_{36}^{E.T} & \varepsilon_{31}^T & \varepsilon_{32}^T & \varepsilon_{33}^T
\end{bmatrix}
\begin{Bmatrix} T_1 \\ T_2 \\ T_3 \\ T_4 \\ T_5 \\ T_6 \\ E_1 \\ E_2 \\ E_3 \end{Bmatrix}
\qquad (1\text{-}9)
$$

1.6 Limitations of Linear Theory of Piezoelectricity

The linear theory of piezoelectricity has limitations in application that are due to different aspects as discussed here

• Electrostriction: The response of piezoelectric materials has a quadratic component which is superposed to the linear theory behavior of the material. This behavior depends on the electrostrictive coefficient which is usually lower than the linear piezoelectric coefficient but always significant as the electric field is increased.

• Depolarization: Piezoelectric materials stay polarized until they are depolarized electrically, mechanically, or thermally.

The exposure of the materials to a strong electric field of opposite polarity will depolarize the material electrically. The field strength needed to depolarize the material depends on the material grade, the length of time the material is exposed to the field and the temperature.

When the mechanical stress on the piezoelectric material is high enough to distort the orientation and alignment of the dipole, the material becomes depolarized mechanically.

Heating a piezoelectric material to its Curie point makes the domains disordered and the materials becomes depolarized completely.

• Frequency limitation: Natural frequency of vibration is available for all physical systems. Exposing the system to a frequency close to the natural frequency of the system will generate an oscillation very high in amplitudes. More linear compliance will be achieved at a frequency far from the natural frequency of the material (Bolaniran, 2021).

CHAPTER TWO
2 LITERATURE REVIEW

This chapter presents detailed literature review of ideas and topics that are related to the research. The different methods of storing energy mechanically are discussed in the chapter. A brief overview of the different applications of piezoelectric materials will be given while a more detailed report on energy harvesting using piezoelectric materials is discussed. This chapter thus provides a basis for the thesis with the presentation of the work and approaches of other researchers while establishing the approach taken for this study.

2.1   Energy Storage

Energy generation and demand are hardly ever balanced. What this means is that there are times when more energy is produced than is demanded and other time, more energy is demanded than can be produced at the time. In addition to this, most renewable energy sources like wind and solar power are erratic this nature cannot be easily controlled. The solution to the above stated problems is energy storage. This allows for energy captured at peak times to be used during down times or when demanded.

Some technologies provide short term energy storage, while others can last for much longer. Common examples of energy storage are the rechargeable battery and the hydroelectric dam. These energy storage devices can be broadly classified into the following methods:

- Mechanical e.g., Compressed air storage, flywheel energy storage and pumped-storage hydroelectricity

- Electrical e.g., capacitors and chemical batteries

- Thermal e.g., Eutectic storage

- Chemical e.g., Biofuels

Each of these have their advantages and drawbacks depending on the mode of use but for the purpose of this research study, mechanical energy storage will be put into focus.

2.1.1 Mechanical Energy Storage

Energy is stored mechanically by using electrical energy to move reversible mechanical systems which hold the energy to be released at a later time. Common examples of energy stored mechanically include, but are not limited to:

- Pumped hydro: Pumped-storage hydroelectricity works by using excess generated electricity during low demand to pump water from a lower source into a higher reservoir. When demand increases, the water is let down to the lower reservoir through a turbine that generates electricity. Reversible turbine-generators act as both pump and turbine. As of March 2012, pumped-storage hydroelectricity (PSH) was the largest capacity form of active grid energy storage. The Electric Power Research Institute (EPRI) reported that PSH accounted for more than 99% of bulk storage capacity worldwide, representing around 127,000 MW. PSH energy efficiency varies in practice between 70% and 80% with some reports claiming efficiency of up to 87% (Energy Storage-Packing Some Power, 2012).

- Compressed air: Compressed air energy storage uses the same principle as PSH. Surplus energy is used to compress air for electricity generation at a later time. The compressed air is stored in an underground reservoir such as a salt dome (Wald, 2010).

- Flywheel: The working principle of the flywheel energy storage (FES) is to accelerate a rotor to a very high speed thereby holding energy as rotational energy. To reduce inefficiency, the system is operated in a vacuum to reduce drag. The flywheel is connected to a motor-generator that interacts with the utility grid through advanced power electronics. Some key advantages are the low maintenance and long life span of the system (Why Energy Storage-Mechanical Energy Storage, 2022).
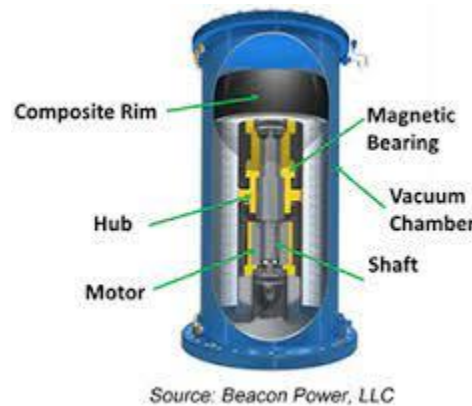
Figure 2-1 Flywheel Energy Storage System

- Springs: Mechanical energy can be stored in power springs. Flat springs are wound up tight and are used to power systems as they unwind. A common implementation of this is the mechanical watches. Springs used to store energy are known commonly as power springs.

2.2   Energy Harvesting

Energy harvesting can be explained as converting energy from one form to another usually more useful form. The energy converted might be energy stored mechanically or chemically, or it could be naturally occurring like wind and solar energy. Although energy

can be harvested in various ways from many different sources, we will focus on energy

harvesting using piezoelectricity for the purpose of this research.

2.2.1   Energy Harvesting using Piezoelectricity

Many piezoelectric materials have been developed over the past century and they have

found widespread use in energy generation due to their ability to output large voltages on

the order of 50 V to 100 V although currents are typically quite small, in the nanoamp to

milliamp range (Safaei, 2019). The majority of piezoelectric energy harvesting transducer

materials aside from PZT and PVDF can be categorized into five groups including

piezoelectric single crystals, lead-free piezoelectrics, high temperature piezoelectrics,

piezoelectric nanocomposites, and piezoelectret foams.

For the energy harvesting efficiency of piezoelectric materials to be optimized, they are

usually incorporated into transducer devices. These devices provide a platform for efficient

mechanical energy absorption based on the energy source and specific application.

The mechanical devices that can be used for this purpose are cantilever, beam, and a

diaphragm. A diaphragm is a mechanical device which is fixed on four ends, while the

cantilever is a mechanical device which is fixed at one end. In the case of beam, two ends

are fixed. Diaphragms and beams are mostly used in piezoelectric sensors.

The piezoelectric cantilever beam configuration (active piezoelectric layer glued on a

passive substrate beam) is the most utilized piezoelectric transducer in vibration energy

harvesting due to its simple structure and convenient fabrication and modeling. The

piezoelectric layer is bonded to a passive substrate to increase the strain in the active

material. In this configuration, the d_{31} piezoelectric strain coefficient is usually used to

convert mechanical vibration to electrical energy. The most common cantilever beam configurations include unimorph (a single piezoelectric layer bonded to a substrate layer) and bimorph (a single substrate layer with two symmetric piezoelectric layers bonded on each side) devices. Piezoelectric beams present a noticeable power generation performance when they are excited at their resonant frequency. Often, an inertial mass is added to the tip of beam harvesters in order to decrease or tune the resonant frequency of the system as well as to improve the mechanical response and output power in low amplitude excitations as seen in Figure 2.1(a) (Erturk, 2009). Using beams with nonrectangular profiles, such as triangle-shaped beams, as seen in Figure 2.1(b) (Goldschmidtboeing, 2008), and trapezoidal cross section beams, the energy output and maximum tolerable excitation of the cantilever harvesters can be improved (Roundy, 2005). In addition, altered mechanical boundary conditions and different beam configurations, including designs with a dynamic amplifier support instead of a fixed end (Figure 2.1(c)) (Park, 2013).
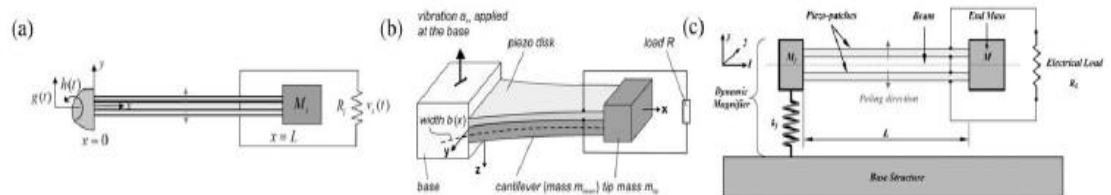
Figure 2-2 Various piezoelectric beam harvesters with (a) tip mass (b) non-rectangular profile (c) dynamic amplifier support (Erturk, 2009)

One issue with cantilever beam energy harvesting is the relatively high resonant frequency and weak energy efficiency of the beams when excited at frequencies below or above the natural frequency.

2.2.1.1 Piezoelectric beams and beam shapes

Cantilever beams are the most commonly used substrates for harvesting energy using piezoelectric materials. This is due to reasons like ease of modelling and the convenience of design. Most energy harvested using piezoelectric material is harvested from natural vibrations and these sources most of the time do not generate a lot of force and the forces generated are erratic. The stress developed on the cantilever is 25 times more than that on a diaphragm and 7 more than that on a beam. Hence, cantilever structure is mostly used to harvest ambient mechanical vibrations, as for some amount of force; it has the capability to produce a significant stress and displacement (Prateek Asthana, 2020). Cantilever beams also have relatively lower natural frequencies. This is important because the natural frequency of the substrate is the optimal operating frequency of the harvester.

The piezoelectric energy harvester efficiency depends on optimizing the cantilever geometry and tuning its natural frequency with vibration source frequency. Beam geometry optimization has been extensively researched and literature shows that adjusting

the shape of the bimorph can significantly affect piezoelectric transduction. The results show that inverted taper in thick and width, inverted taper in thick and inverted taper in width piezoelectric energy harvesters produce 46.15%, 13.13% and 37.70% more power than the conventional rectangular piezoelectric energy harvester. The resonant frequency of inverted taper in thick and width, inverted taper in thick and inverted taper in width energy harvesters is 52.05%, 45.5% and 11.08% lower than the conventional rectangular energy harvester with base excitation (Pradeesh E. L., 2013). However, for tip excitation as is the case with this research paper, other beam shapes aside the traditional rectangular beam create a failure point under continuous operation.

2.3 Piezoelectric Energy Harvesting Devices and Applications

Piezoelectric materials can be used to harvest energy from a large number of sources and applications. Some of these sources and applications are highlighted in this section.

2.3.1 Harvesting energy from airflow

Airflow produces kinetic energy which provide opportunities for piezoelectric energy harvesting. Harvesting energy from wind is more attractive because of its wide availability and its continuous mechanical energy (Yang, 2014). One limitation in wind energy harvesting is the relatively low speed of wind near the ground due to boundary layer effects and physical obstructions such as trees and structures (Kishore, 2014). Airflow is usually harvested using two main device types namely:

Windmill-style harvesters: Wind energy harvesting is usually investigated using this type of harvesters. The original work on piezoelectric energy harvesting using a windmill-style device was presented by Priya et al in 2005 as seen in Figure 3.2(a) (Priya, 2005). Myers et al proposed an optimized windmill harvester with a simpler design shown in Figure 3.2(b) (Myers, 2007). A windmill harvester design was suggested by Tien and Goo in 2010 (Tien, 2010) consisting of a single PZT composite cantilever. A conventional fan with exciter teeth installed on the hub of the turbine was utilized to excite the harvester, as shown in figure 3.2(c). Several researchers have tried to reduce the harvester dimensions and cut-in speed, which will improve the efficiency, by improving the design.

A problem with the windmill designs proposed in this section is that they work at relatively high wind speeds (around 10 mph or 4.5 m s−1), where even conventional electric generators operate efficiently.
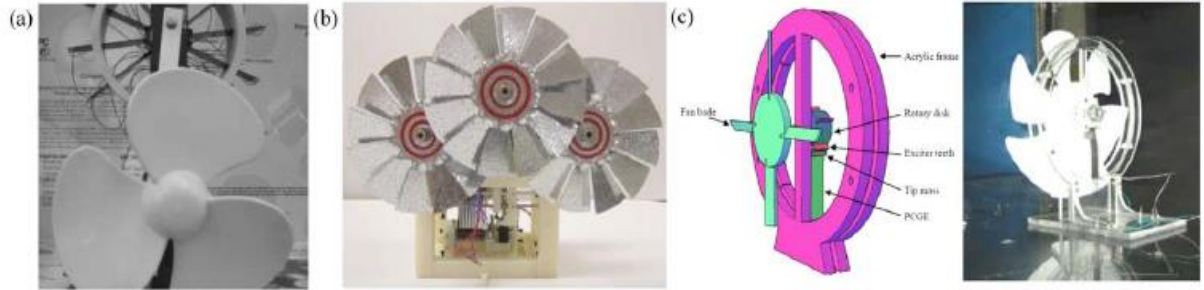
Figure 2-3 Various windmill-style piezoelectric energy harvesters including (a) Priya's harvester (b) Myers's harvester (c) windmill with exciter teeth (Safaei, 2019)

<u>Flutter-style Harvesters:</u> Various flutter-style piezoelectric wind harvesting systems have been developed in the literature including fluttering beams with attached airfoils, wake galloping (a fluttering beam in the wake of a fixed bluff body), and fluttering beams with attached bluff bodies (galloping body). In an initial investigation into flutter-style wind harvesting with an attached airfoil, Tan and Panda in 2007 (Tan, 2007) subjected a piezoelectric beam mounted at an angle to transverse airflow. In order to achieve improved coupling between airflow and the beam, a compliant plastic flapper was installed on the free end of the cantilever. A prototype of the harvester with overall dimensions of $76.7{\times}12.7{\times}2.2$ mm^3 showed a power output of around 155 µW when subjected to an optimal wind speed of 6.7 m s^{-1}. Similar designs of wind harvesters based on the stalk-leaf architecture were proposed by Li and Lipson in 2009 and optimized in 2011 (figure 2.4(a)) (Li, 2011). Experimental test results showed that the cross-flow design could provide significantly more power than the parallel-flow design. A double layered PVDF crossflow long stalk with dimensions of $72{\times}16{\times}0.41$ mm^3 harvested 615 µW power when subjected to 8 m s^{-1} wind speed. Bryant and Garcia in 2011 (Bryant, 2011) expanded upon the work presented by Tan and Panda by developing an aeroelastic

flutter energy harvester containing a rigid flap connected to a piezoelectric cantilever harvester through a ball bearing revolute joint (figure 2.4(b)). A final method of flutter-based energy harvesting involves attaching a bluff body to a piezoelectric beam. Kwon in 2010 [333] developed a galloping body using a T-shaped cantilever beam that facilitates aeroelastic flutter under wind excitation (figure 9(c)).
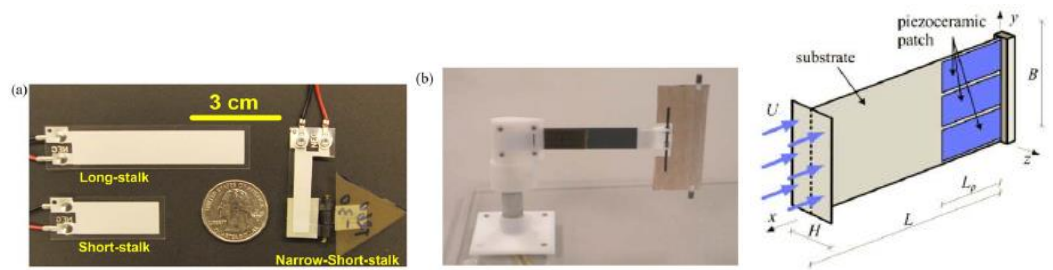
Figure 2-4 Various flutter-style harvesters including (a) flutter stalk (b) flap with revolute joint (c) wake harvester (Safaei, 2019)

2.3.2 Harvesting energy from liquid flow

Research on energy harvesting from liquid flow has been more limited compared to energy harvesting from airflow due to the availability of the source. On the other hand, liquid flow sources, in particular water, can provide continuous energy accompanied with a higher energy density compared to airflow. Taylor et al in 2001 (Taylor, 2001) introduced one of the earliest works on harvesting liquid flow using piezoelectric materials. They presented an energy harvesting eel consisting of a PVDF bimorph emerged in water flow (figure 2.5(a)). A prototype eel with dimensions of 24 cm×7.6 cm×150 μm was fabricated and tested in a flow tank. A peak voltage of around 3.0 V was measured at a water velocity of 0.5 m s^{-1}. In 2014, Xie et al (Xie, 2014) proposed two designs of piezoelectric energy harvesters to generate power from transverse and

longitudinal wave motion. The former harvester was a horizontal piezoelectric cantilever beam attached to a square column on a fixed support under a floating structure (figure 2.5(b)) and the later device was a piezoelectric cantilever column equipped with a tip proof mass (figure 2.5(c)). Analytical modeling results showed that using an optimized design of both devices, an RMS power of 30 W could be generated from the horizontal device with 2.4×1 m^2 cantilever dimension, and 55 W could be generated by the vertical harvester with 3 m cantilever length. Another piezoelectric-buoy energy harvester was proposed by the same research group in 2015 (Wu N. W., 2015) for power harvesting from deep and intermediate ocean waves with relatively higher available power than seabed and shallow waters (figure 2.5(d)).
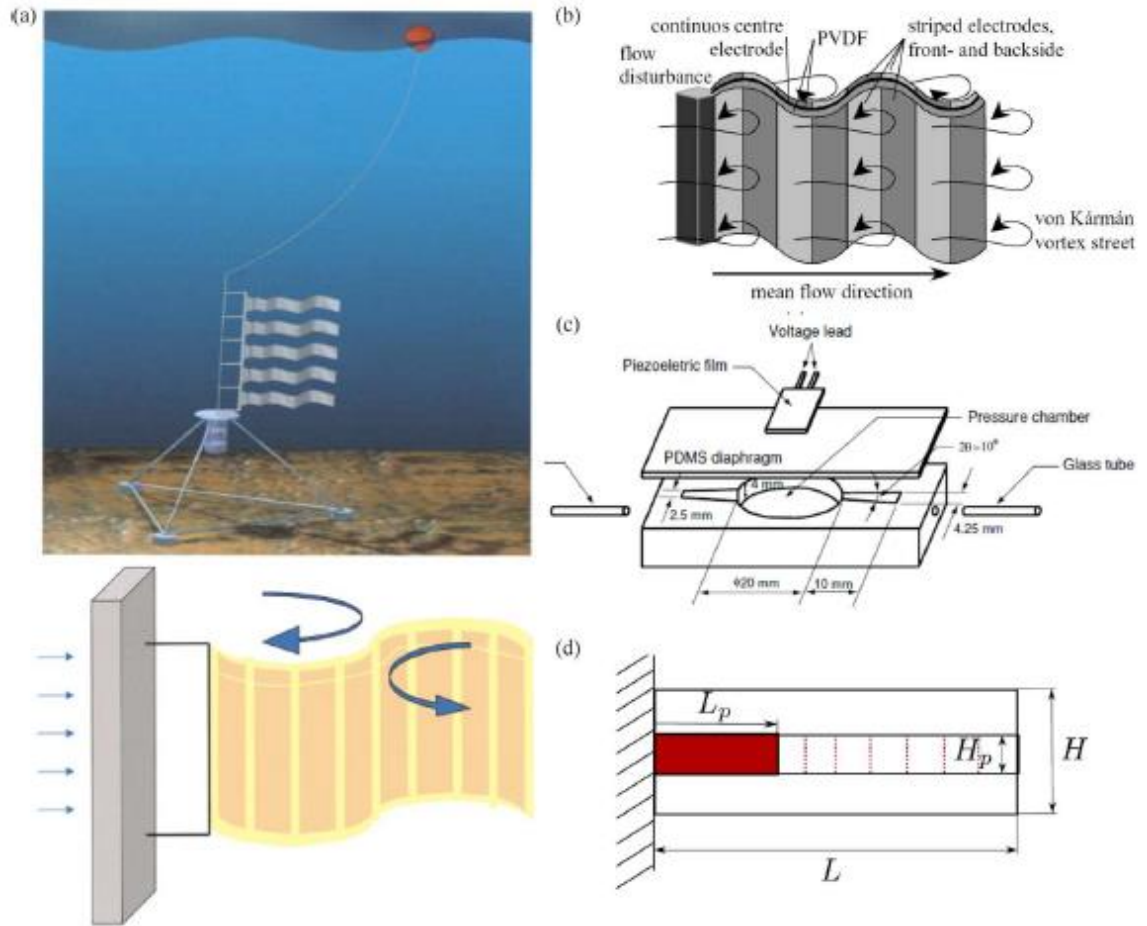
Figure 2-5 Various piezoelectric devices for liquid flow energy harvesting including (a) energy harvesting eel (b) fluttering flag (c) liquid flow pressure fluctuation harvester and (d) sectioned piezoelectric fluttering flag (Safaei, 2019)

2.3.3 Energy harvesting from vibration

Energy harvesting from vibration is one of the most researched aspects of piezoelectric electricity generation. Ju and Ji in 2018 proposed a vibration energy harvester that consists of a spherical proof mass in aluminum housing and a cantilever beam. Maximum peak-to-peak open circuit voltage of 42.2 V and average power of 633.7 µW was obtained at 3 g acceleration at 17 Hz with the single channel and single MFC model fabricated with aluminum housing (Ju, 2018).
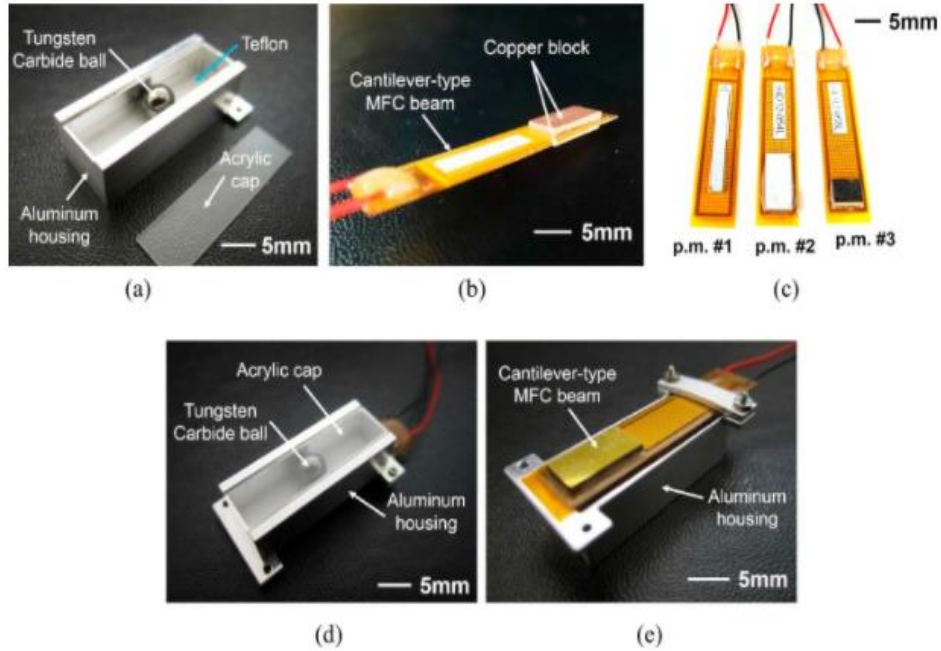
Figure 2-6 Impact-based piezoelectric vibration energy harvester. (Safaei, 2019)

Wu et al proposed and investigated a novel ultra-low frequency and multi-directional piezoelectric energy harvester, based on a simple spring pendulum system. A maximum power of 13.29 mW is obtained for a 2.03 Hz, 0.26 g motion excitation (Wu Y. Q., 2018).
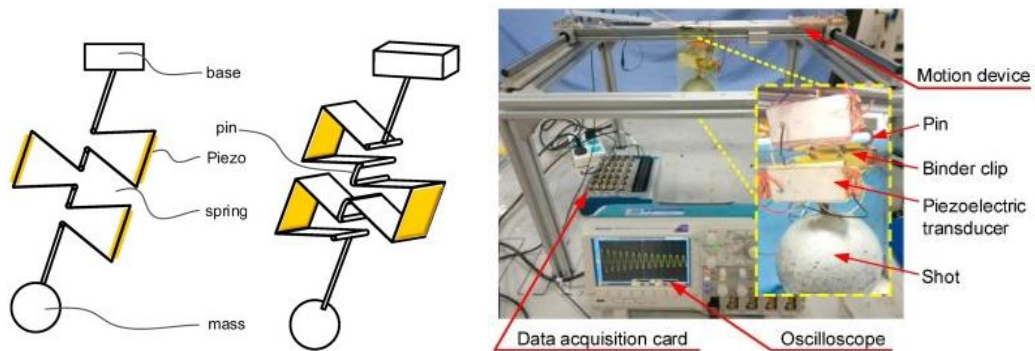
Figure 2-7 A piezoelectric spring pendulum oscillator (Safaei, 2019)

2.3.4 Energy harvesting from vehicles

It has been reported that only 10% to 16% of fuel energy is used to run the car against road friction and air drag. The idea of utilizing the waste energy of cars has led researchers to investigate the feasibility of energy harvesting from the vehicle suspension system and tires, which contain rich vibration and force profiles (Safaei, 2019).
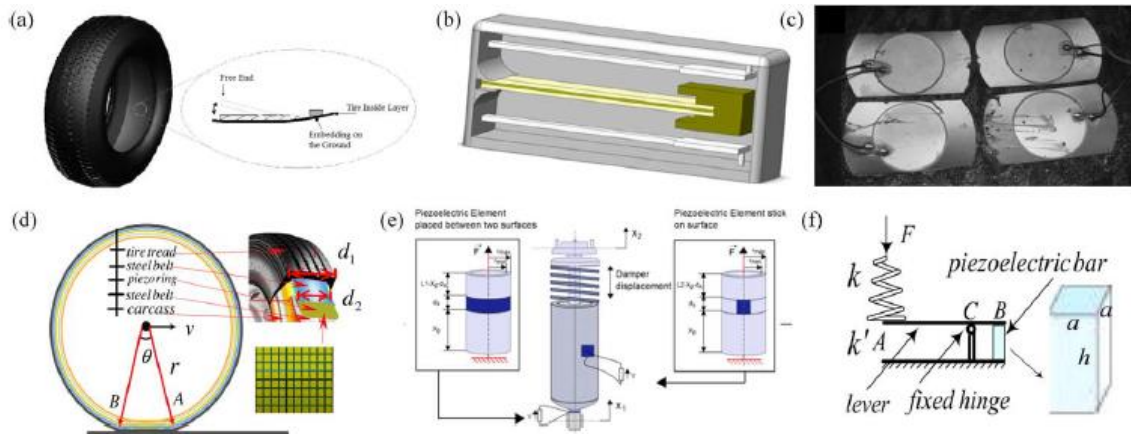
Figure 2-8 Various piezoelectric harvester designs for energy harvesting form vehicles including (a) tire resonant harvester (b) inertial vibrating harvester (c)piezoelectric bender patch (d) tire composite harvester (e) suspension cylinder harvester (f) suspension spring harvester. (Safaei, 2019)

Vehicle suspension systems, which contain high force and mechanical vibration content, have attracted the attention of researchers for implementation of piezoelectric energy harvesting devices in vehicles.

2.3.5 Energy harvesting from springs

In 2008, Frances Hill proposed a system of storing mechanical energy in a CNT spring and generating it using a set of piezoelectric beams. Due to the scaling of the proposed system, the winding of the CNT spring is done by applying an electric charge to the piezoelectric beams and the deformation winds up the spring. The system was proposed

in three different scales all producing an average of 0.0013W, 0.13W and 13W with

varying discharge times with an efficiency between 18-22% (Hill F. A., 2008).

(b)
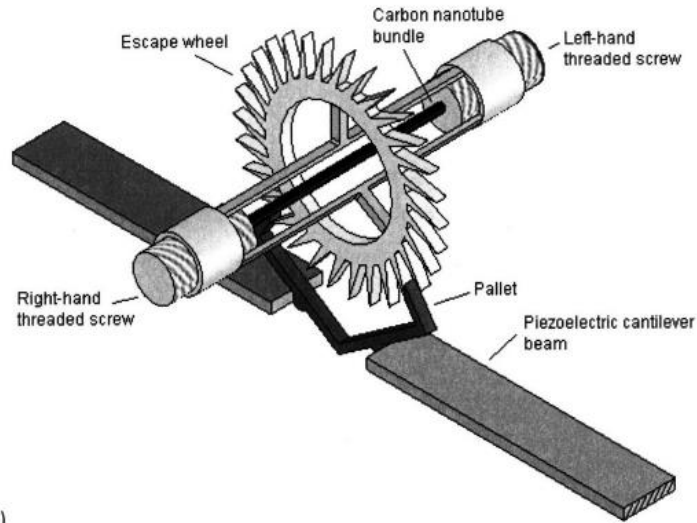
Figure 2-9 Proposed design for the harvester (Hill F. A., 2008)

Hill et al in 2014 proposed a system to harvest electrical energy from mechanical

energy stored in a spring made of CNT. The device makes use of an escapement

mechanism to control the rate of energy released. The device had a run time of 35s

and produced an average output power of 1.nW on an energy conversion rate of

0.01% (Hill F. A., 2014).
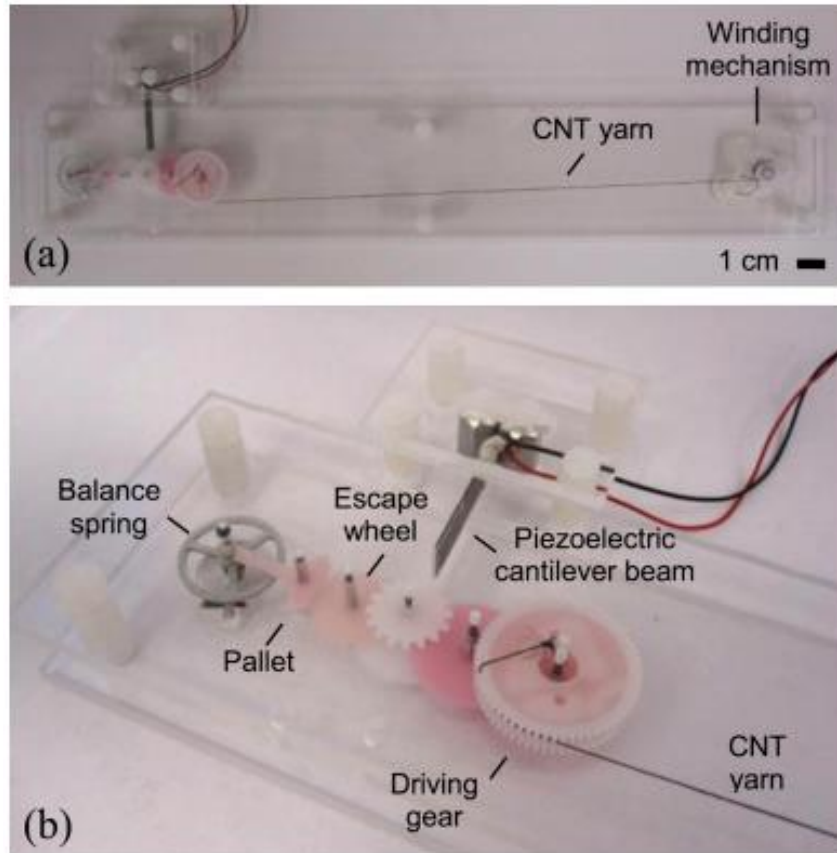
Figure 2-10 CNT battery using a piezoelectric generator showing (a) the entire system (b) a close-up of the power regulation and energy conversion mechanism (Hill F. A., 2014)

2.4   Significance of study

The significance of this research work is to attempt to show how the principles of piezoelectricity can be used in energy generation and harvesting. The goal is to develop a piezo-mechanical battery that stores energy in a power spring and dissipates it slowly using an escapement mechanism. The body of works cited above created the basis for the possibility of achieving this objective by building on the vast work of research that has been done in this field.

CHAPTER THREE

3 THEORETICAL DEVELOPMENT

3.1 Overview

This research is focused on the development of a piezo-mechanical battery. This chapter outlines and discusses the development process. The presentation follows the battery conceptualization and the calculations involved in designing the various components. The implementation of the piezoelectric generator in this application is similar to vibrational energy harvesters that use resonating piezoelectric cantilever beams to generate electrical power with the difference being mechanical energy comes from a spring rather than naturally occurring vibrations.

The design is made of a power spring contained in a barrel that powers the system and also stores energy. The energy stored in the spring is transferred through a gear system to the escapement mechanism that controls the energy release. The escapement mechanism also acts as the power generator. The escapement is the coupling mechanism between the storage element and the generator since its purpose is to convert the energy released from the spring into a form acceptable for input into the generator. Once the spring is fully stretched, the power spring barrel is held in place by a pawl and cam system that restricts it from rotating in the "forward" direction and releasing energy. To discharge energy, the cam is rotated, and the pawl disengages allowing the barrel to turn. The force of the spring turns the gears and eventually, motion reaches the output ring gear, and this turns the escape wheel. As the escape wheel spins, the spring contracts. Without any additional mechanisms, the escape wheel would accelerate and release all of the energy from the spring in a single burst. The role of the pallet is to control the rotations of the escape wheel. The motion of the pallet is driven by the pair of identical cantilever beams that oscillate at

their resonant frequency and have a phase difference of 180 degrees. As the pallet oscillates, it alternately locks the escape wheel in place and then allows it to rotate by a small increment. The escape wheel is locked in place when an escape wheel tooth is in contact with a locking face of the pallet. As the pallet continues its oscillation, an escape wheel tooth comes in contact with an impulse face on the pallet, and the escape wheel is free to rotate. When the escape wheel rotates, it transfers elastic strain energy from the spring through the pallet to the cantilever beams. The energy received by the cantilever beams during each impulse allows the beams to maintain oscillations with large amplitudes over an extended period of time despite damping losses that would otherwise cause the oscillations to die out rapidly. The two cantilevers are coated by a film of piezoelectric material with patterned electrodes above it. As the cantilevers oscillate, the piezoelectric layer converts the stress in the beams into electrical energy. The electrical energy is removed from the system using the electrodes contacting the piezoelectric material.
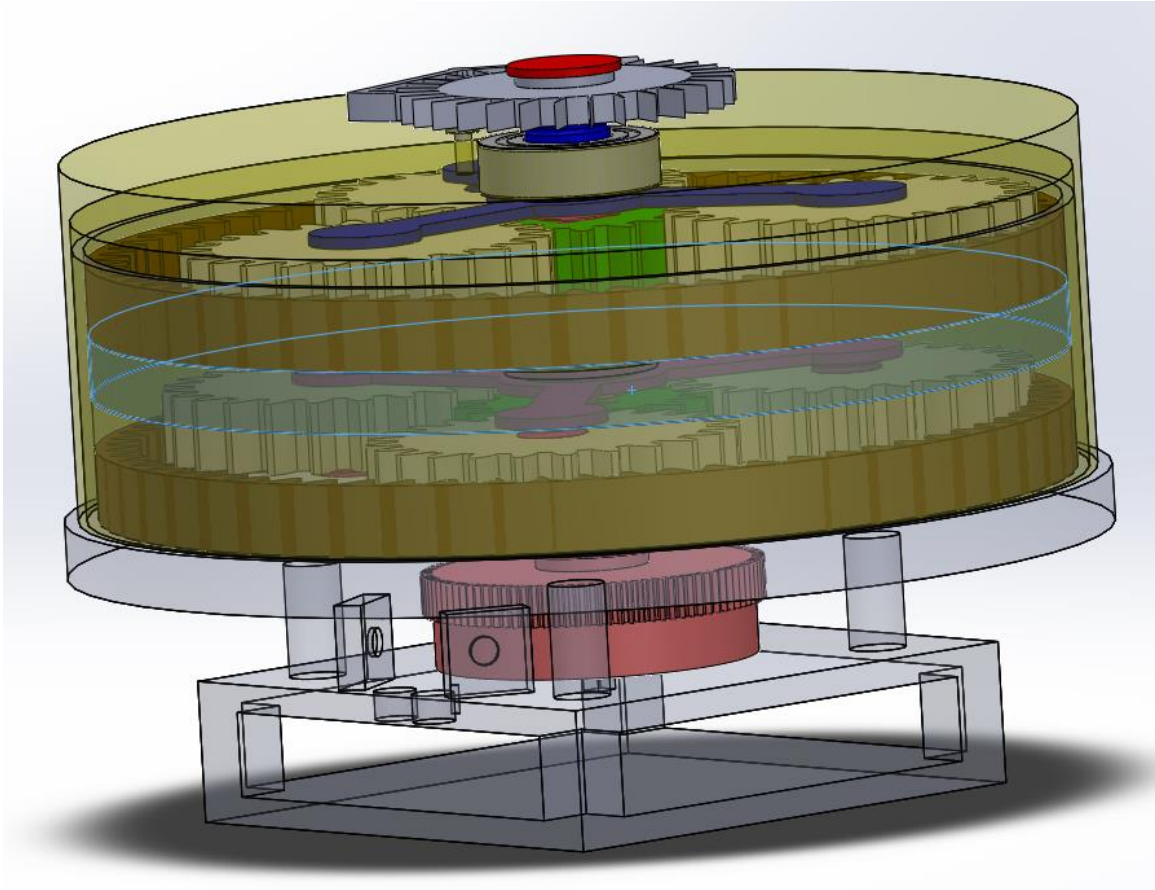
Figure 3-1: Assembly of the piezo-mechanical battery concept.

The system is designed to be reversible. In the normal mode of operation of an escapement,

a moment acting on the escape wheel in the clockwise direction drives the motion of the

pallet. However, if it is the pallet that is driven instead, the oscillations of the pallet drive

the escape wheel in the counter-clockwise direction. In the charging mode of operation, an

alternating voltage applied in the 3 direction to the piezoelectric cantilevers induces

alternating tensile and compressive stresses in the 1 direction, which drives the cantilevers

to oscillate. The oscillations of the cantilevers drive the motion of the pallet, which in turn

rotates the escape wheel in the counter-clockwise direction. This operation stretches the

spring and puts energy into the system for storage. Unimorph cantilevers have been chosen

for the design for their ability to have large displacements, which is useful in the discharging mode of operation. In the charging mode of operation, large forces as well as large displacements are needed for the cantilever beams to overcome the forces from the spring, but piezoelectric bending actuators typically can generate only small forces (Q. Wanf, 1999). The maximum forces required of the cantilever beams and the required applied voltages needed to reach these forces to fully stretch a spring will be examined in more detail in the system model.

3.2   Battery concept and configuration

The concept of a battery is a device that can store energy in one form and convert the stored energy to electrical energy when needed. With the goal of the research in mind, it was easy to filter through the different forms of energy storage and select springs as the better option. The energy density of springs (about 0.1 Wh/kg for steel) is not as high as it would need to be for large scale energy storage applications, it is enough for MEMs applications. The device consists of a power spring, a gear system for motion transfer, an escapement mechanism to control the release of energy and a set of piezoelectric beams to harvest the energy. Most of the initial design criteria came from the size constraint. The research focused on making the battery as portable as could be. The device was made of 3D printed PLA to reduce the amount of inertia in the moving parts as not a lot of force is being generated by the stainless steel spring.

3.3   Energy storage and power source

The spring in this device can serve as a storage for energy or as a source of power depending on the direction the device is being run. One of the best examples of a device that works with a similar operation is the mechanical watch or clock. The power spring of

a mechanical watch is stored in a component known as the mainspring barrel. The power

spring is attached to the inside wall of the barrel on one end and to a spring arbor on the

other end. The function of the spring arbor is to hold down the spring and ensure that the

only way the spring can unwind is to turn the barrel itself thereby releasing energy into the

system.

The dimensions of the mainspring barrel were arbitrarily selected based on the relative size

of the other components of the PMB. The teeth on the outside of the barrel are there for the

pawl and cam system that controls the direction of the barrel motion during the charging

or discharging of the system.

The spring arbor is made to connected to the rest of the base and not rotate. Only the main

barrel moves. The barrel cover is designed to also be a shaft for the first gear in the gear

system. The shaft on it attaches to the sun gear and the gear turns as the barrel turns. This

serves to transfer energy to the system.

Given the dimensions of the barrel and the power requirements, the dimensions of the

spring can be chosen.

The spring constant, k is calculated as

$$k = \frac{Ebt^3}{12l} \qquad (3\text{-}1)$$

where E is the longitudinal elastic modulus of the material the spring is made from, b is the

material width, t is the plate thickness, and l is the total length of the spring.

The stress when any moment occurs on the spring is calculated as

$$\sigma = \frac{6M}{bt^2} \qquad (3\text{-}2)$$

and M is the moment which is equivalent to the torque delivered per turn and is calculated as

$$M = 2\pi k \qquad (3\text{-}3)$$

The total torque delivered by the power spring is calculated by multiplying the torque per turn by the number of turns of the spring in the barrel. The number of turns is calculated as

$$T = \frac{\sqrt{2-(D^2+d^2)}-(D+d)}{2t} \qquad (3\text{-}4)$$

Where D is the internal diameter of the barrel, d is the outside diameter of the arbor, and t is the thickness of the spring. The force produced by the spring drops off sharply in the final turns. This creates what is known as "lost turns". Therefore, the effective or working turns in the barrel is 1.5 turns less the actual number of turns. (Boettcher, 2006)

3.4   Gears and Gear System

Energy generated by the spring has to be transferred to the piezoelectric cantilever beam to be harvested and turned into electricity. Much like a mechanical watch or clock, a gear system is used in this device to transmit motion. The choice of gears and system is based on the criteria of highest gear ratio and compactness of design. The high gear ratio leads to a longer run time of the device and the compactness of the design adds to the portability of the battery.

The easiest set of gears and gear system to design and fabricate are spur gears. Spur gears are ones in which the teeth are parallel to the axis of the gear (Norton, 2012).

In order to get a train ratio greater than about 10:1 with spur gears, it is necessary to compound the gear train or an epicyclic gear system. Compound gears with very high gear

ratios contain many gears or very large gears and as earlier stated, the size of the device is a major constraint. The solution to this problem is to make use of an epicyclic or planetary gear train. Conventional gear trains are one-degree-of-freedom devices but epicyclic gear trains are two-DOF devices and two inputs are required to obtain a predictable output. Epicyclic gear trains provide high load capacity and compactness to gear drives. Simple epicyclic planetary gear trains with a stationary ring gear have a ration range between 3:1 and 9:1. For similar epicyclic gear trains with compound planet gears, the practical gear ratio range varies from 8:1 to 30:1. For the purpose of this research, the device needed to have a higher gear ratio and using differentia-planetary gear arrangements would make it possible (Kapelevich, 2014).

3.4.1 Two-stage compound epicyclic gear train

The gear train design for the battery is a two-stage compound epicyclic drive. In the first stage of this drive, the sun gear is the driver. The annulus or ring gear is held stationary as part of the base and the carrier arm is the driven component. The sun gear of the second stage is attached to a shaft connected to the carrier arm and this drives the second stage. In the second stage, the sun gear is once again the driver, and the annulus is held stationary. The final output of the drive is the second stage carrier. The corresponding gears of the two stages all have the same number of teeth. Therefore, the gear ratio of the train is calculated by squaring the formula for calculating the gear ratio in epicyclic drives.

$$u = \left(1 + \frac{N_a}{N_s}\right)^2 \qquad (3\text{-}5)$$

Where N_a is the number of teeth of the annulus and N_s is the number of teeth of the sun gears.

3.4.2   Gear sizing and formulas

The *American Gear Manufacturing Association* (**AGMA**) defines standards for gear design and manufacture. They define a spectrum of quality numbers and tolerances ranging from lowest to highest (3-16).
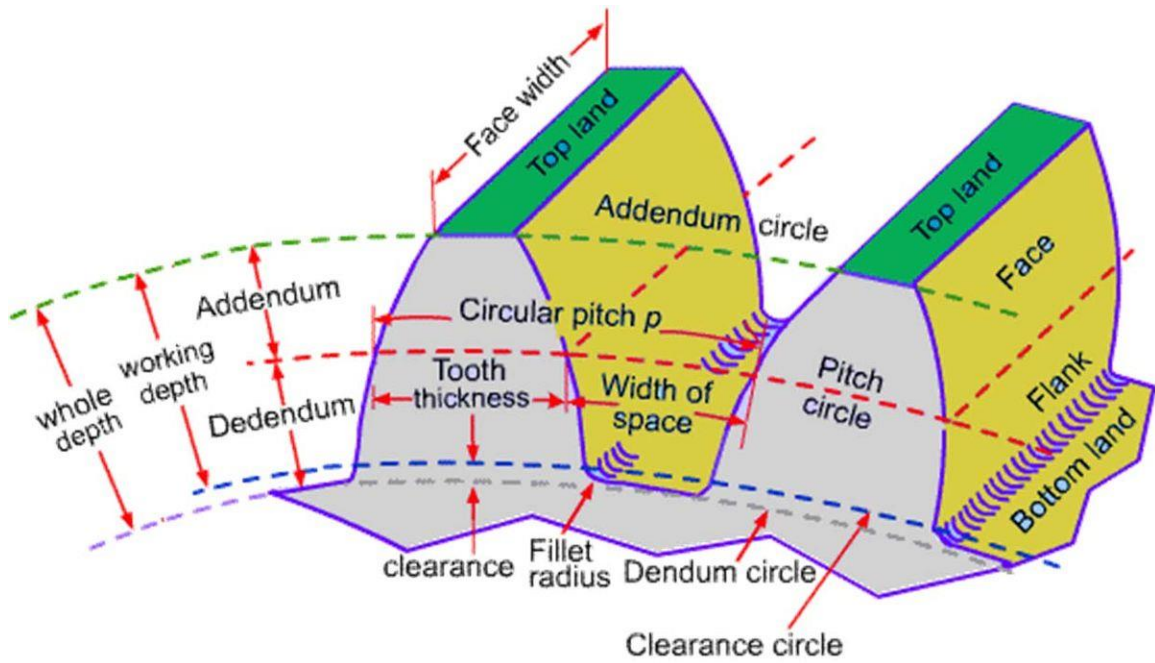
Figure 3-2 Gear tooth nomenclature

Parameter	Coarse Pitch ($p_d < 20$)	Fine Pitch ($p_d \geq 20$)
Pressure angle ϕ	25° or 25°	20°
Addendum a	1.000 / p_d	1.000 / p_d
Dedendum b	1.250 / p_d	1.250 / p_d
Working Depth	2.000 / p_d	2.000 / p_d

Whole depth	2.250 / p_d	2.200 / p_d + 0.002 in
Circular tooth thickness	1.571 / p_d	1.571 / p_d
Filler radius-basic rack	0.300 / p_d	Not standardized
Minimum basic clearance	0.250 / p_d	0.200 / p_d + 0.002 in
Minimum width of top land	0.250 / p_d	Not standardized
Clearance (shaved or ground teeth)	0.350 / p_d	0.350 / p_d + 0.002 in

Table 3.1 AGMA Full-Depth Gear Tooth Specifications

The other tooth dimensions are standardized based on the table above. The circular pitch p_c is

$$p_c = \frac{\pi d}{N} \qquad (3\text{-}6a)$$

where d is the pitch diameter and N is the number of teeth. The tooth pitch can also be measured along the base circle circumference and is called base pitch p_b

$$p_b = p_c cos\phi \qquad (3\text{-}6b)$$

A more common way to define tooth size is to relate it to the diameter of the pitch circle. The diametral pitch p_d

$$p_d = \frac{N}{d} \qquad (3\text{-}6c)$$

Combining equations 3-9a and 3-9c gives the following relationship between circular pitch and diametral pitch.

$$p_d = \frac{\pi}{p_c} \qquad \text{(3-6d) (Norton, 2012).}$$

Using the above mentioned formulas, the gear system of the system was calculated and designed.

3.5   Escapement mechanism

One of the main objectives of the research is to be able to control the rate of energy release from the power spring. While the simplest way to release energy from a spring is a quick burst of energy, this application requires steady flow of energy.

An escapement mechanism is a set of carefully designed gears whose rotation is controlled by an oscillator (Hill F. A., 2008). The escapement mechanism is made of three main components: am oscillator, an escape wheel, and a pallet. As the mainspring unwinds, it drives the escape wheel, a gear with specially designed gear

teeth, to rotate. The pallet is a gear that is used to control the mainspring's rate of unwinding via the escape wheel. The motion of the pallet is driven by the oscillator. Through precise interlocking of the pallet and escape wheel teeth, each successive oscillation of the pallet allows the escape wheel to advance by an angle corresponding to a single gear tooth. The pallet has two locking faces and two impulse faces, as shown in Figure 3.5. When a locking face of the pallet is in contact with an escape wheel tooth, the escape wheel is held stationary and prevented from rotating. As the pallet continues its rotation, an impulse face of the pallet comes into contact with an escape wheel tooth and the escape wheel becomes free to rotate. As the escape wheel rotates, it pushes against the impulse face of the pallet,

and the elastic energy released from the spring gets transferred through the escape wheel
and the pallet to the oscillator. This event is called an impulse.
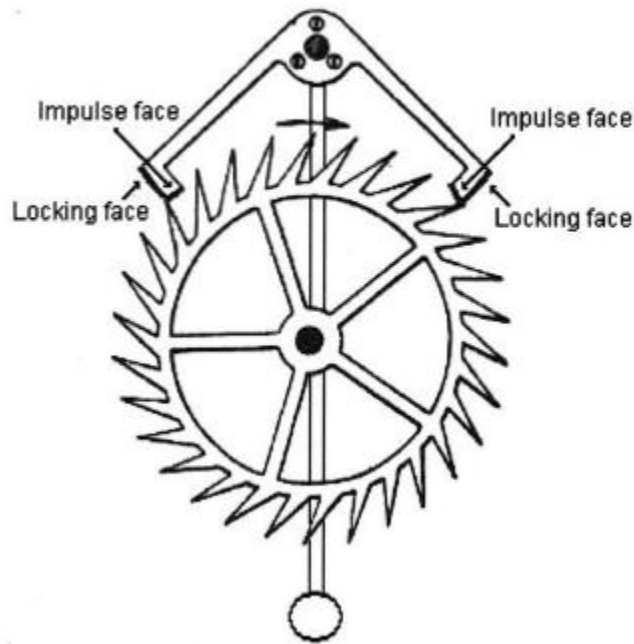
Figure 3-3 Diagram of a deadbeat escapement showing the impulse faces and locking faces of the pallet

3.5.1 Escapement Design

For the design of the escapement mechanism, a dead beat escapement, or Graham escapement, has been adopted since it is commonly used in pendulum clocks and is well understood.

The geometry of the pallet and escape wheel are discussed in detail. First, a circle of radius R is drawn. The radius of the circle can be chosen to be any convenient length. A second circle of radius 3/4R is drawn inside the first circle. A radius of the larger circle is drawn. A line is drawn that forms a 6° angle with the radius, passing through the point of

intersection between the radius and the outer circle. A second line is drawn that forms a

12° angle with the radius, passing through the same point of intersection. These steps are

shown in Figure 3.6 (a). The two angled lines form the first escape wheel tooth. To draw a

second tooth, a second radius is drawn 12° from the first radius. Once again, two lines are

drawn that make 6° and 12° angles with the radius line, passing through the point of

intersection between the radius and the outer circle. These two lines form the second tooth.

This process is repeated by rotating the radius each time by 12°, until 30 teeth have been

drawn. The completed drawing of the escape wheel is shown in Figure 3.6 (b) with

construction lines shown as dotted lines.
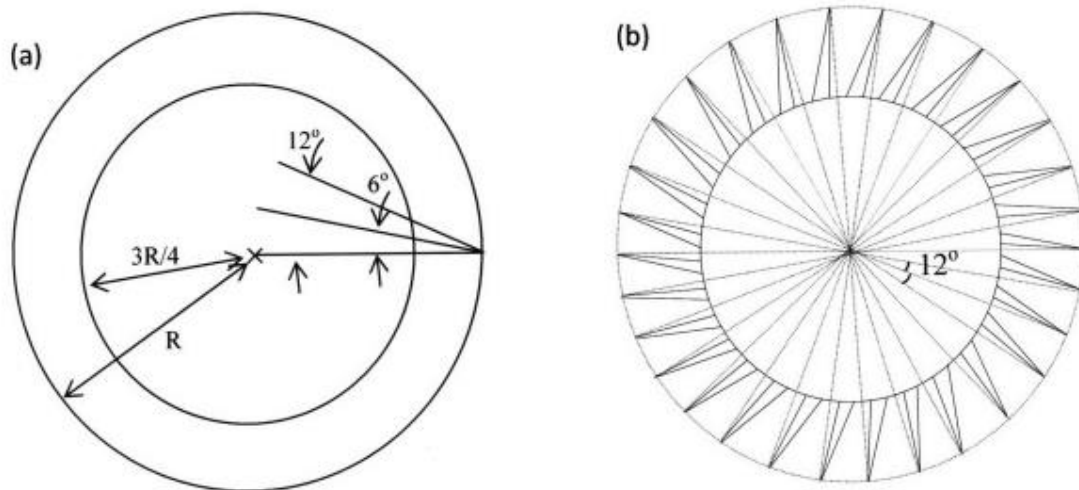
Figure 3-4: Construction lines used to draw the escape wheel teeth. (Hill F. A., 2008)

Once the escape wheel has been drawn, the next step is to add the pallet. A line is drawn

through the center of the escape wheel circle and extended to form a centerline. Two radii

of the circle are drawn perpendicular to each other, at 45° angles to the centerline, above

and below it. A second circle with a radius of R is drawn so that its center lies on the

38

centerline, and it passes through the two points of intersection between the first circle and

the two perpendicular radii. The centers of the circles are separated by a distance of $\sqrt{2}$R.

Two perpendicular radii of the second circle are drawn to the two points of intersection of

the circles. The lines of all four radii are extended for construction purposes. Next, 8

additional lines are drawn that are 3° to either side of the four radii and pass through the

centers of the circles. These construction steps are shown in Figure 3.7.
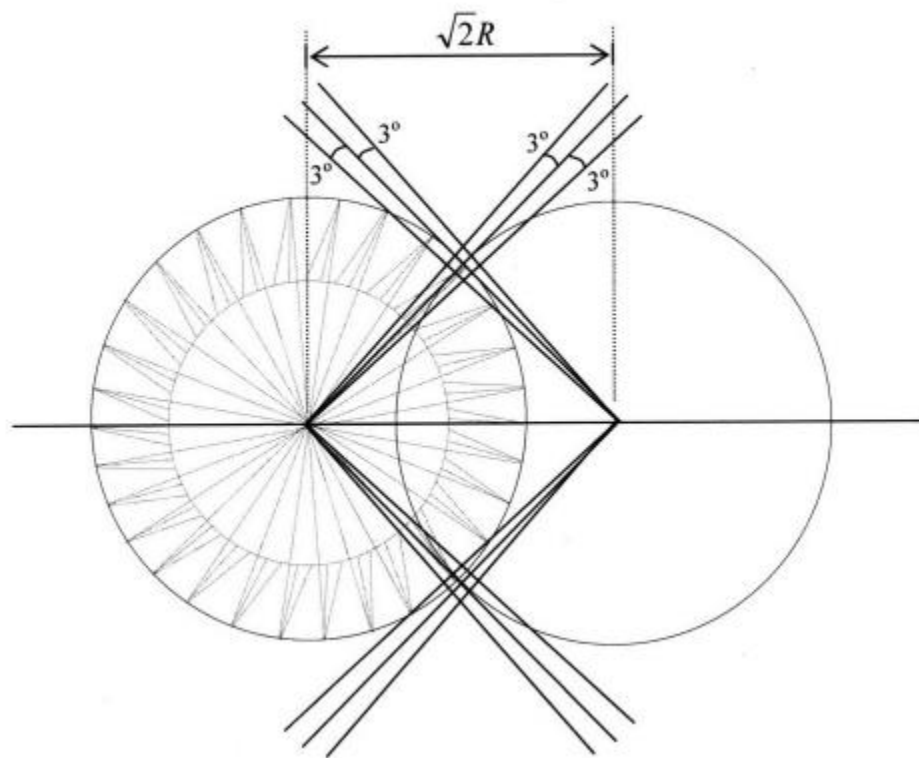
Figure 3-5: Construction lines for drawing the pallet. (Hill F. A., 2008)

To form the locking faces of the pallet, vertical and horizontal lines are drawn through the

intersections of these extended lines. Next, two more concentric circles are drawn about

the center of the pallet circle. These two circles have radii lengths of 0.952*R and 1.057*R.

A diameter of the pallet circle is drawn perpendicular to the centerline. Two pallet arms

construction lines are drawn at an angle of 24° to this diameter through the center of the circle. An additional two lines are drawn to the right and left of each of the two pallet arm construction lines at a distance of 0.04R, and it is these four lines that form the pallet arms. These steps are shown in Figure 3.8.
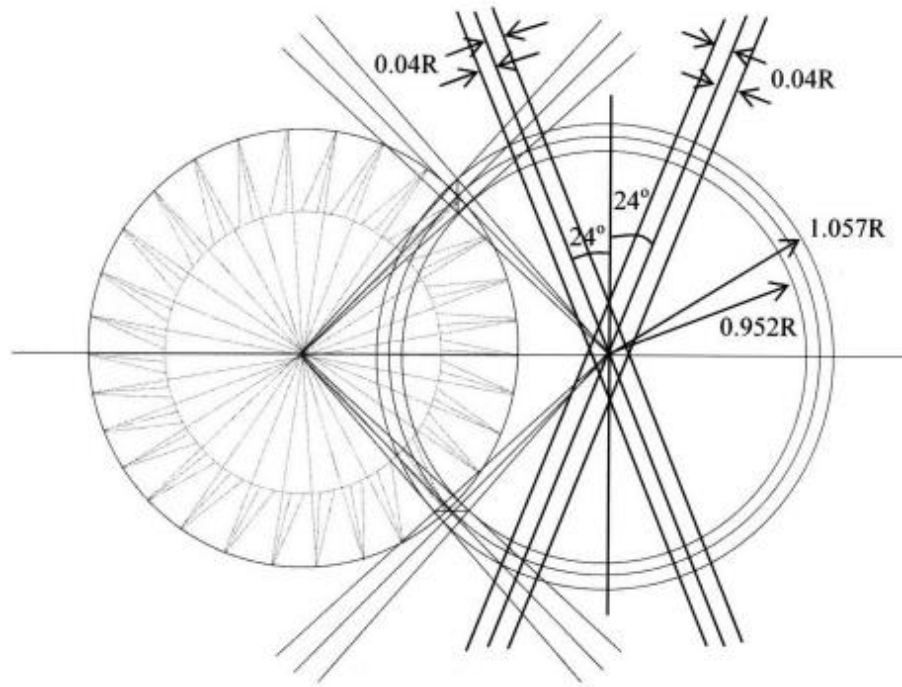
Figure 3-6: Construction lines to form the pallet (Hill F. A., 2008)

The construction of the deadbeat escapement is complete, and the next step is to remove all construction lines. The resulting diagram is shown in Figure 3.9. The last step is to finish the detail on the escape wheel and the pallet.
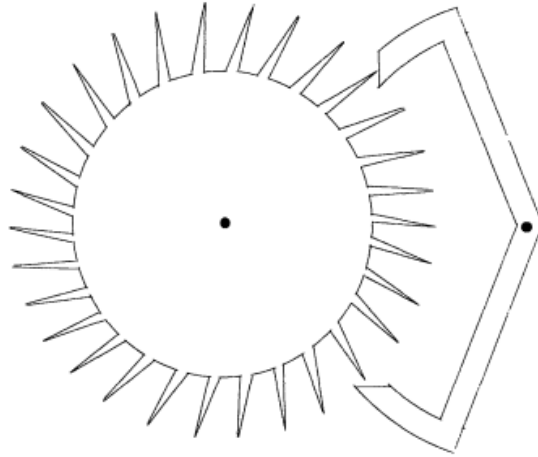
Figure 3-7: Escapement with all construction lines removed. (Hill F. A., 2008)

3.5.2 Escapement modelling

The escapement mechanism in this research is modeled similar to an escapement mechanism in the research done by Frances Hill in 2008 (Hill F. A., 2008). The geometry of the pallet and the two cantilever beams is shown in Figure 3.10. The pallet arms have length R. The cantilevers are placed underneath the pallet arms and contact each arm at its midpoint. In the neutral position, the tips of the cantilevers contact the pallet at a vertical height of h_o and a horizontal distance of b_o from the center of rotation of the pallet. In the neutral position, the pallet arm forms an angle θ_o with the horizontal axis so that $b_o = \frac{r}{2}cos\theta_o$ and $h_o = \frac{r}{2}sin\theta_o$. The design requires that the pallet and the cantilever tip displace together so that the cantilever drives the motion of the pallet. When a pallet arm is moving downwards, it will press down on the tip of the cantilever beam, constraining the cantilever tip to move with the pallet. The angle of displacement of the pallet with respect to its neutral position is denoted as $\theta_p(t)$ and the tip displacement of the cantilever beam is denoted as $x(t)$, where both functions of time, and these two variables are related with a simple

41

approximation. Using the geometry of Figure 3-8, the pallet angle and the cantilever tip displacement are related by

$$\theta_p(t) = tan^{-1}\left(\frac{h_o + x(t)}{b_o}\right) - \theta_o \qquad (3\text{-}7)$$
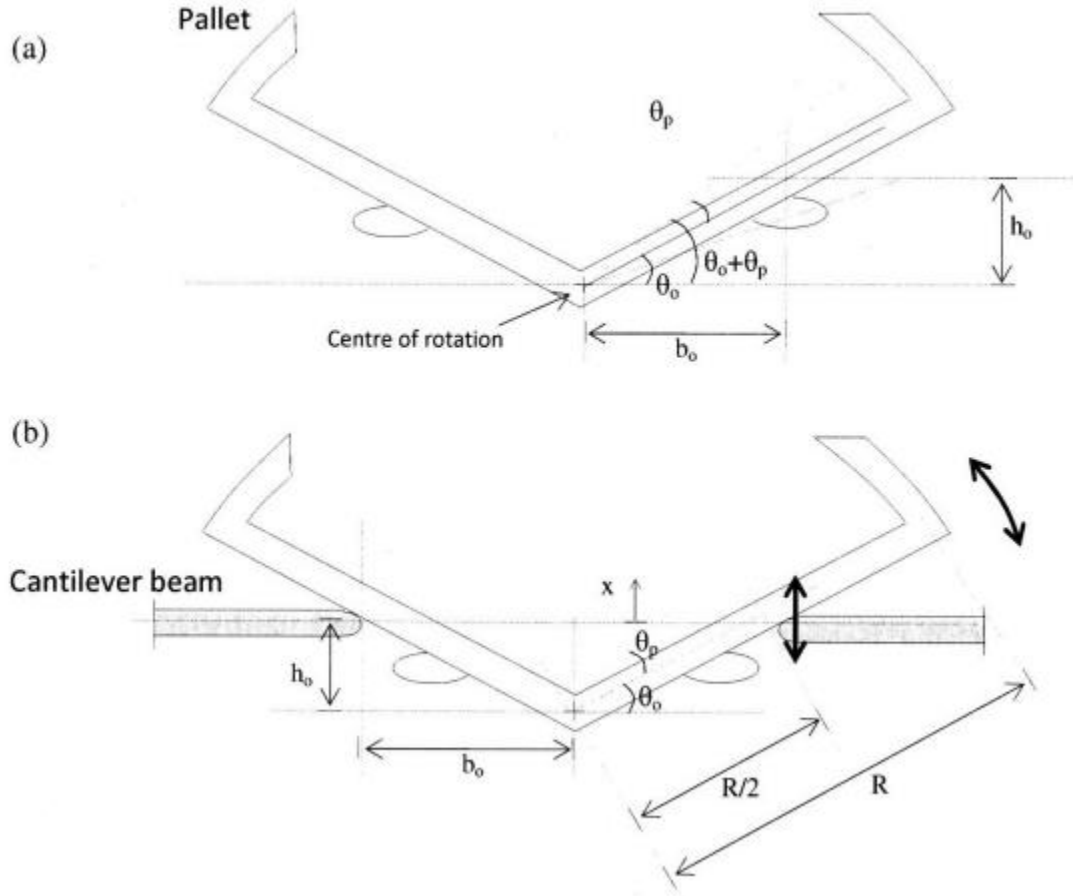
Figure 3-8: (a) Geometry of the pallet. (b) Diagram showing the geometry and connection between the pallet and the cantilever beams (Hill F. A., 2008)

Together, the escape wheel, pallet and cantilever beams form a mass-spring-damper system. The spring functionality is provided by the two cantilever beams. Damping in the system is a result of mechanical losses and the piezoelectric conversion of energy from the mechanical to the electrical domain. The overall damping coefficient is modeled as a sum

of the mechanical damping coefficient b_m and the electrical damping coefficient b_e. The mass functionality comes from the inertia of the cantilevers, pallet, and escape wheel. Finally, the spring provides the driving force in the system which is transferred to the mass through the escape wheel mechanism.

Each beam is modeled as a tip loaded cantilever. The cantilevers have length L, height H and width W. The effective mass m_{eff} of each cantilever is calculated as $m_{eff} = \frac{33}{140} \times m_{beam}$, where $m_{beam} = \rho \times LWH$ is the actual mass of the cantilever beam and ρ is the density of the material of the cantilever. A spring constant of $k = \frac{EWH^3}{4L^3}$ ia assigned to the cantilevers, where E is the Young's modulus of the cantilever material.

Free body diagrams are used to show the forces acting on the escape wheel, pallet and cantilevers during an impulse or locking phase. During an impulse, the pallet and the escape wheel rotate by $6°$ by design. They are constrained to move together and have the same angular velocity. In the free body diagram of the escape wheel, E_x and E_y are the reaction forces at the escape wheel's pivot at point E. M is the moment driving the escape wheel to rotate due to the spring. F_p is the normal force exerted by the pallet on the escape wheel tooth. In the free body diagram of the pallet, P_x and P_y, are reaction forces at pallet's pivot at point P, F_p is the force exerted by the escape wheel tooth on the pallet impulse face, and F_{c1} and F_{c2} are the forces exerted by the cantilever beams on the pallet. In the free body diagram of the cantilever, F_{c1} is the force exerted by the pallet on the cantilever and F_k and F_b represent the damping and spring forces acting on the cantilever.

Figure 3-9: Free body diagrams showing the forces acting on the escape wheel, pallet, and cantilevers during an impulse. (Hill F. A., 2008)

In the diagram, θ_p is the angle of rotation of the pallet with respect to its neutral position and x is the vertical displacement of the cantilever tip. Also, θ_w is the total angle of rotation of the escape wheel with respect to its starting position prior to the release of the spring. The following equations are obtained from the free body diagrams:

$$\text{Wheel: } \sum M_R = -F_P R \cos 45 + M = I_w \ddot{\theta}_w \qquad (3\text{-}8)$$

$$\text{Pallet: } \sum M_P = F_P R \cos 45 - F_{c1} \frac{R}{2} - F_{c2} \frac{R}{2} = I_P \ddot{\theta}_P \qquad (3\text{-}9)$$

$$\text{Cantilevers: } \sum F_x = -kx - (b_m + b_e)\dot{x} - F_{c1}(\theta_o + \theta_P) = m_{eff} \ddot{x} \qquad (3\text{-}10)$$

Because the escape wheel and pallet have the same angular velocity and acceleration, $\dot{\theta}_w = \dot{\theta}_p$ and $\ddot{\theta}_w = \ddot{\theta}_p$. Combining the equations gives the equation of motion

$$m_{eff} \ddot{x} + (b_m + b_e)\dot{x} + kx = \left[M - (I_w + I_p)\ddot{\theta}_w \right] \frac{\cos(\theta_o + \theta_p)}{R} \qquad (3\text{-}11)$$

In the locking phase, an escape wheel tooth is in contact with the locking face of the pallet so that the escape wheel cannot rotate.

Escape wheel   Pallet F_p Cantilever

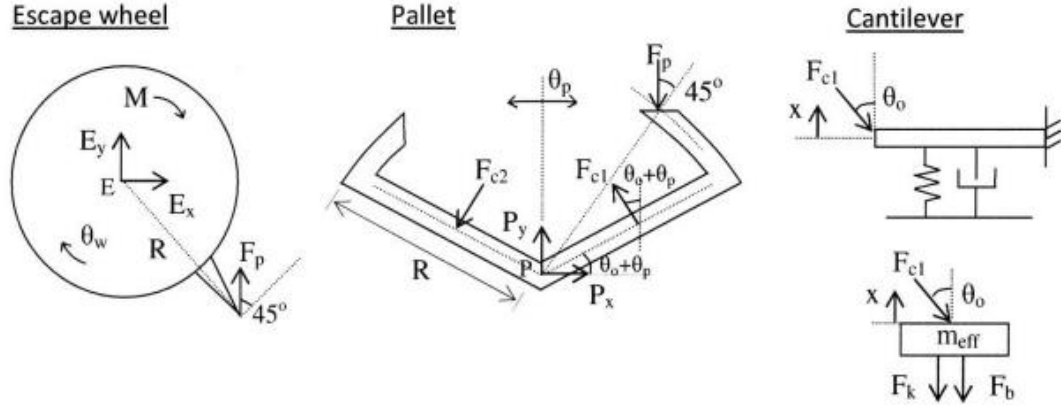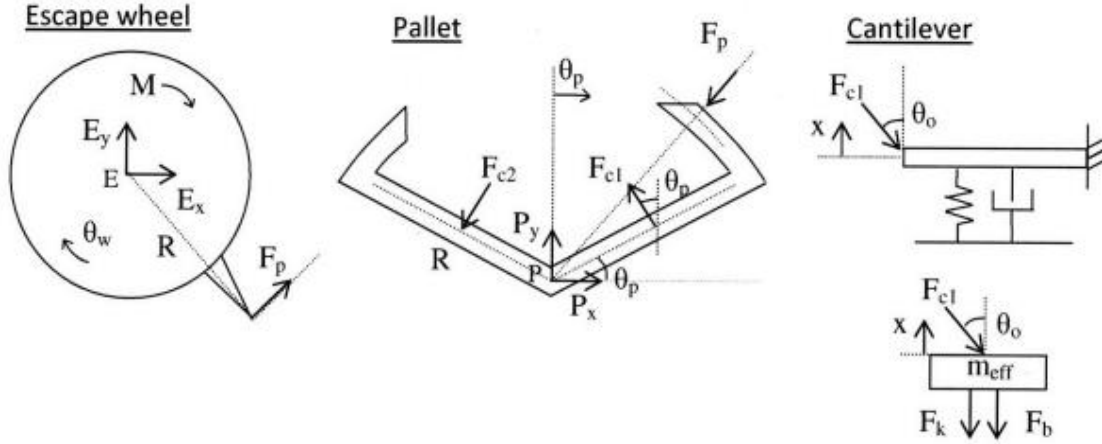*Figure 3-10: Free body diagrams showing the forces acting on the escape wheel, pallet, and cantilevers between impulses. (Hill F. A., 2008)*

The following equations are obtained from the free body diagrams:

$$\text{Wheel: } \sum M_R = -F_P R + M = 0 \qquad (3\text{-}12)$$

$$\text{Pallet: } \sum M_P = F_P R \cos 90 - F_{c1}\frac{R}{2} - F_{c2}\frac{R}{2} = I_P \ddot{\theta}_P \qquad (3\text{-}13)$$

$$\text{Cantilevers: } \sum F_x = -kx - (b_m + b_e)\dot{x} - F_{c1}(\theta_o + \theta_P) = m_{eff}\ddot{x} \qquad (3\text{-}14)$$

Combining the equations gives the equation of motion

$$m_{eff}\ddot{x} + (b_m + b_e)\dot{x} + kx = \left[-I_p\ddot{\theta}_p\right]\frac{\cos(\theta_o + \theta_p)}{R} \qquad (3\text{-}15)$$

Where $\theta_p(t) = \tan^{-1}\left(\frac{h_o + x(t)}{b_o}\right) - 30°$ and $\dot{\theta}_w = 0$.

In summary, for this escapement design, an impulse will occur for $-3° < \theta_p < 3°$ and the escape wheel is locked for $\theta_p > 3°$ and $\theta_p < -3°$. The motion of the pallet is described as

$$m_{eff}\ddot{x} + (b_m + b_e)\dot{x} + kx = \left[-I_p\ddot{\theta}_p\right]\frac{\cos(\theta_o + \theta_p)}{R} + U(\theta_p) \times \left[M - I_w\ddot{\theta}_w\right]\frac{\cos(\theta_o + \theta_p)}{R} \qquad (3\text{-}16)$$

Where $U(\theta_p) = 1$ for $-3° < \theta_p < 3°$ and $U(\theta_p) = 0$ otherwise.

3.6   Cantilever beams

Like most of the device, the piezoelectric beams are 3D printed and made of PLA. Because the unimorph cantilever beams are part of the escapement mechanism as well as the energy harvester, the dimensions of the beam have been carefully selected.

The arm of the pallet is approximately 1 inch long and $\frac{1}{4}$ inch wide. The length of the spring was selected as 2 inches and $\frac{1}{4}$ inch wide. The natural frequency of a cantilever beam is calculated as

$$\omega = (\beta l)^2 \sqrt{\frac{EI}{\rho A l^4}} \qquad (3\text{-}17)$$

Where βl is the mode shape constant for a fixed-free boundary condition. Setting the frequency to 30Hz, the thickness of the beam is found to be 0.5 inches. The spring constant of the beam is calculated as

$$k = \frac{3EI}{l^3} \qquad (3\text{-}18)$$

3.7   Device Runtime

Estimating the device runtime is important for calculating the power generated. By design, the escapement turns $12°$ per oscillation. This translates to 30 oscillations per revolution. With a beam frequency of 30Hz, the number of effective turns and the gear ratio, the runtime is approximated to 2.5 minutes.

3.8   Design Assumptions

Piezoelectric materials especially ceramics with thicker dimensions are anisotropic in nature. They possess properties that are of different values at different direction. Since this

study was performed with a piezoelectric film having a thin thickness, it is assumed that the properties of the film used one dimensional and that they are the same across all spatial direction and the beam theory can be applied.

It is also assumed that the developed strain in the substrate is transferred directly unto the film without absorption or altering by the adhesion material between the film and the substrate. This assumption is necessary to approximate the energy harvested by the system.

Losses in the system are also assumed to be negligible and therefore not considered in the scope of the research.

CHAPTER FOUR
4 NUMERICAL AND EXPERIMENTAL VALIDATION

In this chapter, the numerical and experimental validation of the battery designed in chapter three is presented. A detailed description of the materials employed as well as their properties, the reasons behind those choices and the simulation tools used in validating the output numerically are discussed in this chapter. This stage of the study is necessary because we need to use simulation tools available to confirm that the methods used as well as the assumptions made when developing the battery are acceptable before we proceed to construct the sensor for experimental validation.

The piezo-mechanical battery designed in the previous chapter was 3D printed in ABS filament. This method of production was chosen for its relative cheapness and the ease of production. However, it cannot withstand the forces and power needed to produce a substantial amount of power from the PVDF film. The scope of the project was thereby split into two phases. In one phase, the concept of the battery's mechanism and its reversibility was proven and in the next phase, the voltage and power generated by and unimorph cantilever beam in a clamped-free boundary condition was measured. The piezo-mechanical battery concept can therefore be fabricated with stronger materials and a more spring employed to generate the needed force to produce adequate voltage and power.

4.1   Numerical Validation
4.1.1   Formulas

Researchers have studied the behavior of piezoelectric materials under different working and boundary conditions for a long time. According to research conducted by Roundy et al in 2003 (S. Roundy, 2003), the certain parameters and output can be approximated using

a simplified model for piezoelectric power generation. The frequency of operation is dependent on the dimensions of the cantilever beams the piezoelectric film is attached to. The beam dimensions affect the spring constant and natural frequency of the beam. Damping also varies depending on the load driven by the beams and the structure of the beam. The mechanical damping, b_m cannot be known without measuring the performance of the system, but it can be approximated using quality factor values. The electrical damping b_e is calculated as

$$b_e = 2m\zeta_e w \qquad (4\text{-}1)$$

where

$$\zeta_e = \frac{wk_{31}^2}{\sqrt{w^2 + 1/(R_L C)^2}} \qquad (4\text{-}2)$$

And C is the capacitance of the piezoelectric layer, R_L is the external load resistance, and w is the angular frequency of the cantilever oscillations. Using the simplified model for piezoelectric power generation discussed in the study, the e electrical power generated by a single piezoelectric cantilever beam is equal to the power removed from the mechanical system due to the electrical damping,

$$P = \frac{1}{2} b_e \dot{x}^2 \qquad (4\text{-}3)$$

The total energy harvested from the system over the running duration of the device is approximated as

$$E = 2 \times \int_{t_{end}}^{t_{start}} \frac{1}{2} b_e \dot{x}^2 dt \qquad (4\text{-}4)$$

As with any mechanical system, there are losses associated with the energy harvesting. Frictional losses in the gears, energy lost due to the escapement design and losses in the piezoelectric effect are some of the losses. For the purpose of the research, the losses are assumed to be negligible. Therefore, the efficiency of the system is calculated as

$$\eta = \frac{2 \times \int_{t_{end}}^{t_{start}} \frac{1}{2} b_e \dot{x}^2 dt}{U} \qquad (4\text{-}5)$$

where U is the strain energy stored in the spring and is calculated as

$$U = \frac{1}{6} E \mathcal{E}^2 \qquad (4\text{-}6)$$

Here $\mathcal{E}$ is the maximum allowable strain and E is the Young's modulus of the material the spring is made from (Hill F. A., 2008).

The charge density and voltage output can be estimated numerically as well. In their study in 2020 (J.R. Leppe-Nerey, 2020), discovered that piezoelectric film made from PVDF and PMMA with a 70/30 ratio by weight has slightly better performance while being cheaper than pure PVDF films. From the results of the research, the charge density C_σ is calculated as

$$C_\sigma = \frac{C}{A} \qquad (4\text{-}7)$$

where C is the electric charge induced by the piezoelectric effect onto a surface area A of the material. The electric charge is calculated with the equation

$$C = d_{31} \sigma A \qquad (4\text{-}8)$$

and d_{31} is the piezoelectric coefficient and σ is the stress on the piezoelectric film via the beam substrate calculated as

50

$$\sigma = \frac{Mc}{I} \qquad (4\text{-}9)$$

Here M is the moment about the neutral axis of the beam, c is the perpendicular distance

from the surface to the neutral axis and I is the moment of inertia. To measure the voltage

output, the circuit has to be closed using a resistor whose value is numerically determined

using the formula

$$R = \frac{1}{C\omega} \qquad (4\text{-}10)$$

where C is the capacitance of the piezoelectric material and ω is the natural frequency of

the beam substrate (Hill F. A., 2014).

In order to run the system in reverse and "charge" the battery, a voltage is applied to the

piezoelectric cantilevers to drive their oscillations. For a unimorph cantilever subject to an

applied external force F at the tip and an applied voltage V, the tip displacement δ is (Q.

Wang, 1999)

$$\delta = aF + bV \qquad (4\text{-}11)$$

where

$$a = \frac{4s_{11}^E L^3}{W t_p^3} \frac{AB+1}{1+4AB+6AB^2+4AB^3+A^2B^4} \qquad (4\text{-}12)$$

$$b = \frac{3d_{31}L^2}{t_p^3} \frac{AB(B+1)}{1+4AB+6AB^2+4AB^3+A^2B^4} \qquad (4\text{-}13)$$

Here $A = \frac{E_m}{E_p}$, $B = \frac{t_m}{t_p}$, L is the beam length, W is the beam width, t_m is the thickness of the

cantilever substrate layer, t_p is the thickness of the piezoelectric layer, E_m is the Young's

modulus of the substrate layer and E_p is the Young's modulus of the piezoelectric layer. The pallet has to drive through a known distance δ while supporting a force calculated as

$$F_{c,max} = \frac{M_{max}}{Rcos45} \qquad (4\text{-}14)$$

where M_{max} is the maximum moment on the spring. Maximum voltage required to wind the spring is calculated using

$$V_{max} = \frac{\delta + aF_{max}}{b} \qquad (4\text{-}15)$$

4.1.2   Material selection and dimensions

The spring used in the battery is made of carbon-steel and the dimensions are shown in the table below

Parameter	Dimension	Units
Length, l	1.8	Meters
Width, w	0.015	Meters
Thickness, t	0.0015	Meters
Number of turns	4.5	turns
Young's modulus, E	2.06e11	N.m^{-2}
Spring constant, k	0.4828	N.m/rad
Torque, M	9.1	N.m

Table 4.1: Spring dimensions

The piezoelectric material chosen for this research is the PolyVinyliDene Fluoride (PVDF). PVDF is chosen as our choice of material because it is highly flexible and easily shaped to obtain the desired form for the purpose of this research. The silver ink metallization option of the PVDF is used for this research.

Symbol	Parameter	PVDF	Units
t	Thickness	9, 28, 52, 110	Mm
d_{31}	Piezo Strain Constant	23	$10^{-12} \frac{m/m}{V/m} \ or \ \frac{C/m^2}{N/m^2}$
d_{33}		-33	
g_{31}	Piezo Stress Constant	216	$10^{-3} \frac{V/m}{N/m^2} \ or \ \frac{m/m}{C/m^2}$
g_{31}		-330	
k_{31}	Electromechanical Coupling Factor	12%	
k_t		14%	
C	Capacitance	380 for 28 μm	pF/cm^2 @ 1KHz
E	Young's modulus	2-	10^9 N/m^2
V_o	Speed of Sound: Stretch	1.5	10^3 m/s

	Thickness	2.2	
P	Pyroelectric Coefficient	30	10^{-6} C/m^2 K
ε	Permittivity	106-113	10^{-12} F/m
$\varepsilon/\varepsilon_0$	Relative permittivity	10-12	
ρ_m	Mass Density	1.78	10^3 kg/m
ρ_e	Volume Resistivity	$>10^{13}$	Ohm Meters
Y	Yield strength	45-55	10^6 N/m^2
T	Temperature Range	-40-100	°C
V_{max}	Maximum Operating Voltage	750	V/μm

Table 4.2: Properties of PVDF film

The beam substrate material for the battery is PLA. The dimensions and properties are presented in the table below

Parameter	Symbol	Value	Unit

Length	L	0.0508	Meters, m
Width	b	0.00635	Meters, m
Thickness	h	4.15e-4	Meters, m
Density	ρ	1240	kg/m^3
Modulus of elasticity	E	3.6	GPa

Table 4.3: Beam substrate properties

With an estimated maximum allowable strain of 0.005 for carbon steel and a Young's modulus of 210 GPa, the strain energy density of 875 kJ/m^3 using eqn(4-6). With a density of carbon-steel of 7800 kg/m^3, this corresponds to an energy density by mass of 111 J/kg.

The gear ratio for the gear system of the battery is calculated using eqn (3-5) to be approximately 55:1.

For the second phase of the project, aluminum is used as the beam substrate. The substrate is needed to serve as a support for the film and for the strain developed to be transmitted to the PDVF film. The substrate is of the fixed-free boundary condition, and this is the boundary condition on which the theoretical development is based. The dimensions and properties of the beam substrate are as presented in Table 4.4

Parameter	Symbol	Value	Unit
Length	L	0.1016	Meters, m

Width	b	0.0254	Meters, m
Thickness	h	1.5875e-3	Meters, m
Density	ρ	2700	Kg/m^3
Yield strength	Y	145	MPa
Modulus of elasticity	E	68.9	GPa

Table 4.4: Dimensions of beam substrate

4.1.3 Finite Element Analysis and Simulation

After all parameters were chosen and the system was designed, ANSYS was used to test the components of the system that will be subjected to high stress to ensure they will not fail under said stress.

Following the flow of force from the source, we can see that the spring arbor is the first component that is subjected to a moment. The function of the spring arbor is to prevent the spring from unwinding from its center. This forces the spring to turn the drive shaft. The spring used in the battery has a maximum torque of 0.08 Nm (0.73 lbf in). The arbor was modelled in ANSYS and subjected to the maximum moment with the appropriate boundary conditions and material properties.
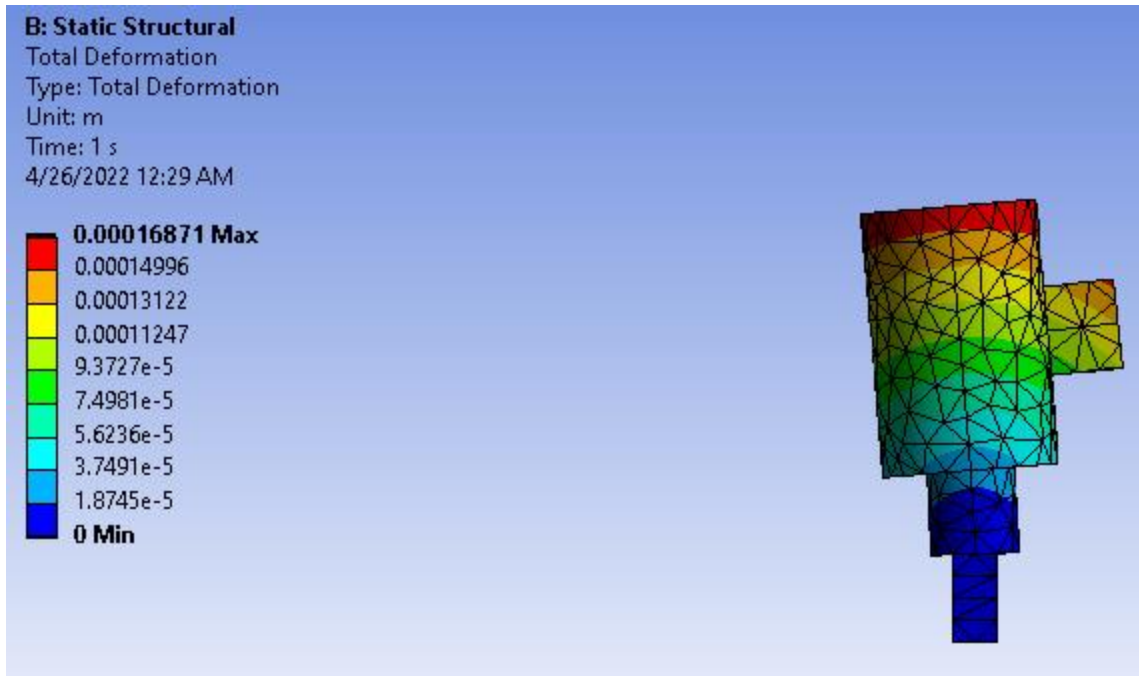
Figure 4-1: Total deformation of the spring arbor subjected to 0.08 Nm of moment

Figure 4-2: Safety factor of the arbor under maximum moment.

On the opposite side of the force floe are the piezoelectric beams. Finite element analysis

was carried out on the beams to ensure the can withstand the output force of the gear train

while still deflecting enough to run the escapement mechanism. The minimum deflection required to run the escapement mechanism is calculated as 3.35mm and from the results of the analysis, the beams deflect without failing.
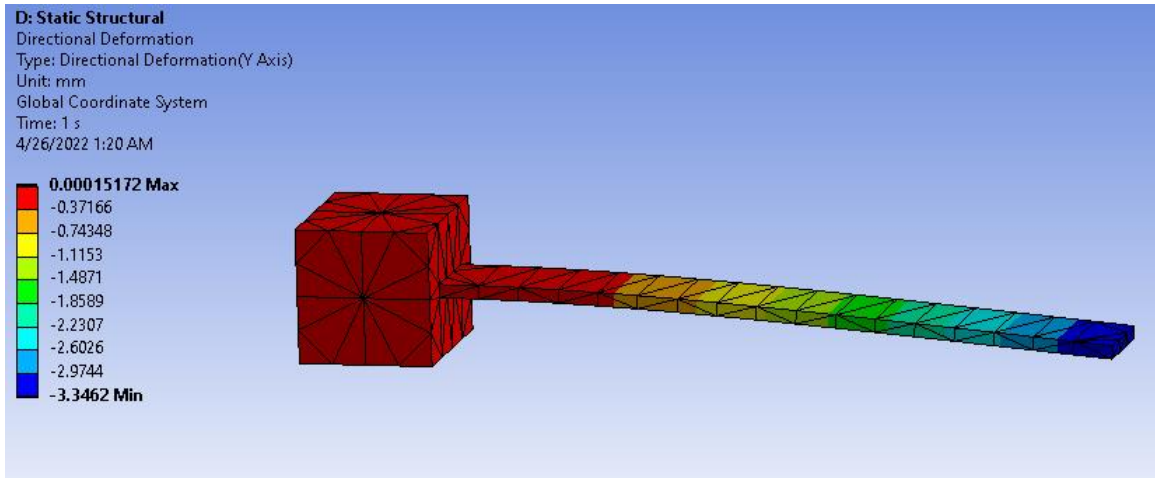

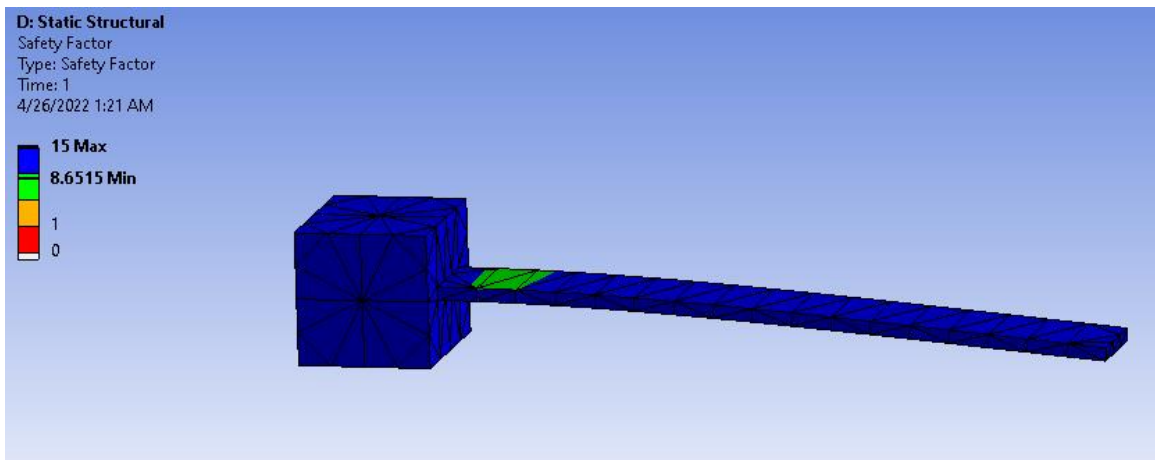*Figure 4-3: Directional deformation of the beam in the Y axis.*

Figure 4-4: Safety factor of the beam .

Finite element analysis was also used to estimate the voltage and current produced in the second phase of the project. ANSYS piezoelectric and MEMs toolbox was used to apply boundary conditions and apply forces. Through ANSYS, the natural frequency of the beam

was obtained. This is necessary to calibrate the recording device and accurately record the results of the experiment.
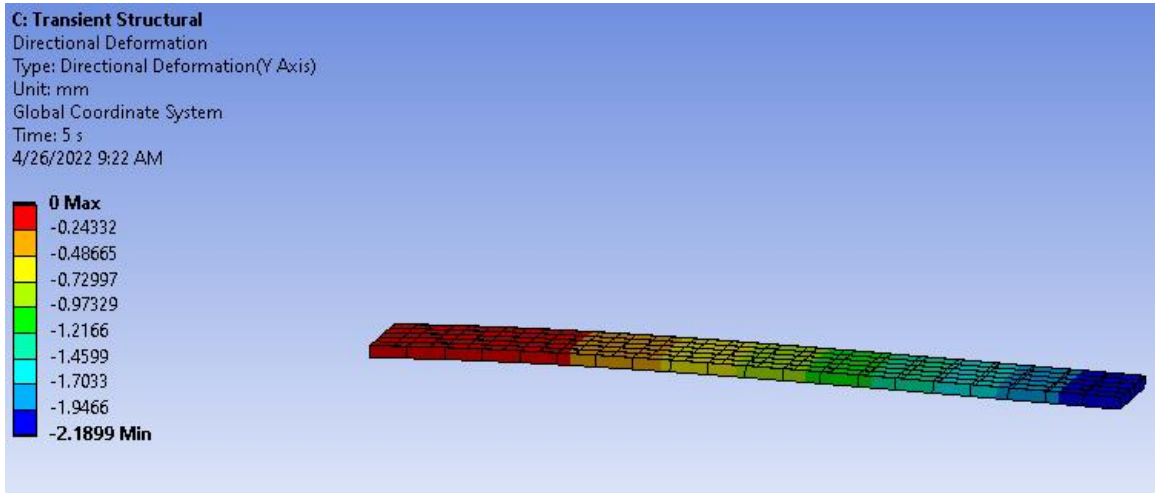

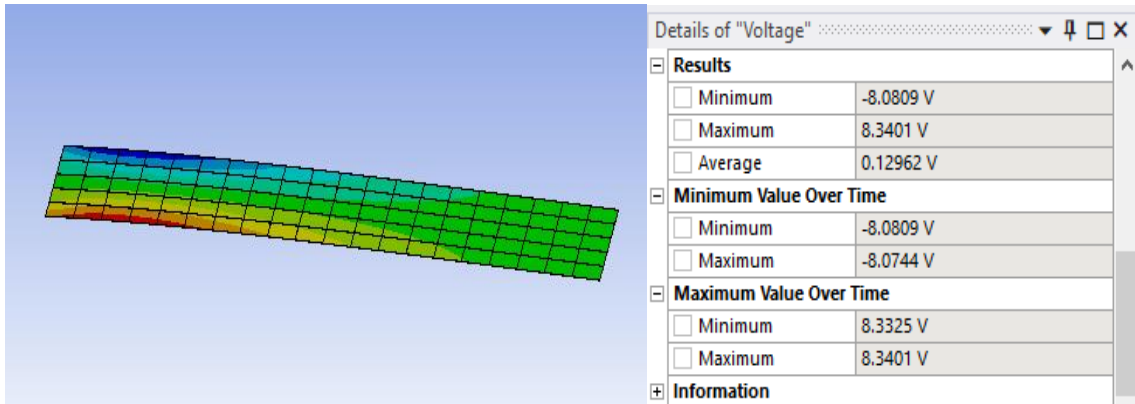*Figure 4-5: Deflection of the aluminum beam under 12N of force*

Figure 4-6: Voltage distribution on the PVDF film under 12N of force. An average of 0.13 volts was generated by the film.
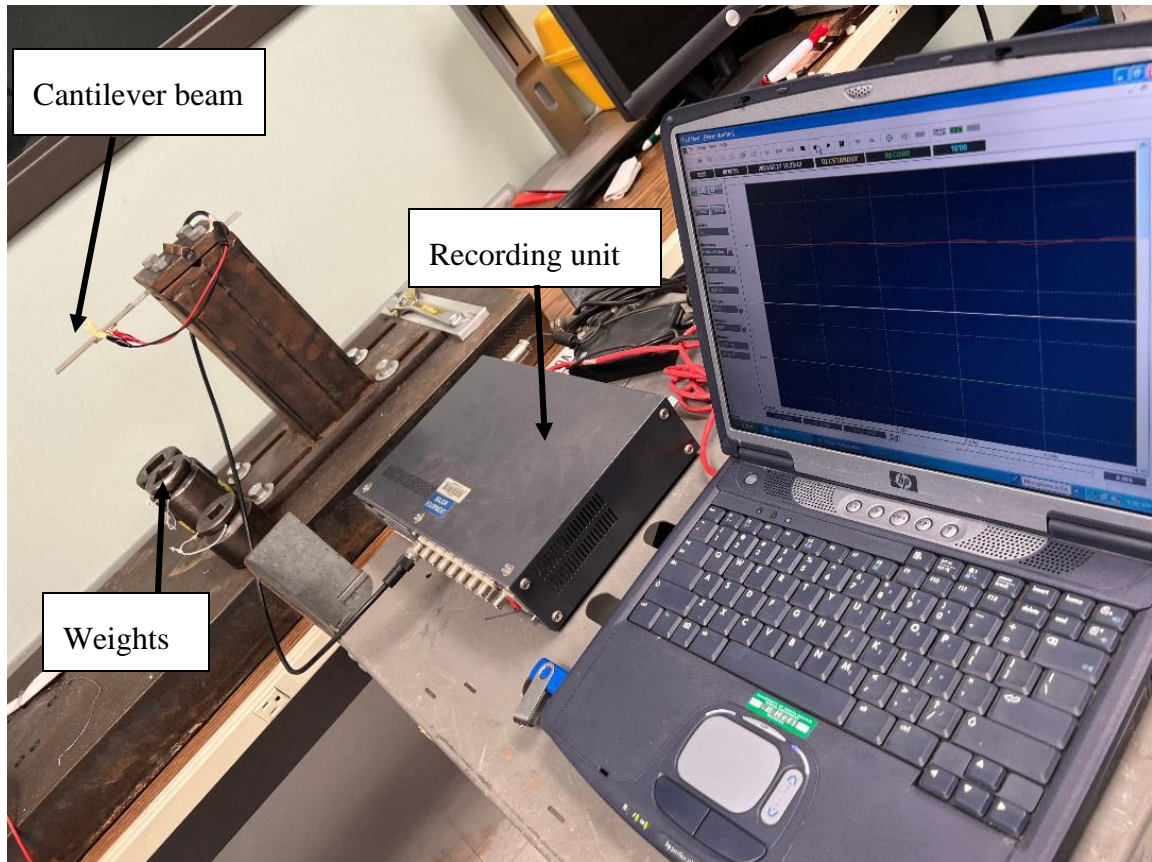
4.2   Experimental validation

In this phase of the research, the simulation results of the piezoelectric beam is attempted to be confirmed. The apparatus and process are described below.

Apparatus: Wrench, clamp, aluminum cantilever beam, PVDF film, thread, hook and weights, scissors, probes, potentiometer, DAQ system.

*Figure 4-7: Data acquisition system.*

Figure 4-8: Experiment setup

<u>Procedure:</u>

- Using the wrench, the cantilever beam is held firmly in the clamp with the required length of 4 inches on the free end.

- The PVDF film is cut to the required size and attached to the beam using adhesive. A tab is left for the attachment of the probes.

- The probes are attached to the tab and connected to the DAQ system.

- A loop is created using the thread and hung at the free end of the unimorph cantilever beam.

- The hook and appropriate weight are hung from the thread loop. The weight is calculated using the formula F=Mg, where g is the acceleration due to gravity.

61

- The thread is then cut, and the beam allowed to vibrate freely.

- The voltage generated by is measured using the DAQ system.

- To measure current as the output, the procedures are repeated but the circuit is closed with the potentiometer.

Expected results: The expected results are voltage and current being measured by the DAQ system and the value being the same or close to the values obtained from the numerical analysis with minimal error.

Breadboard with potentiometer forming closed circuit
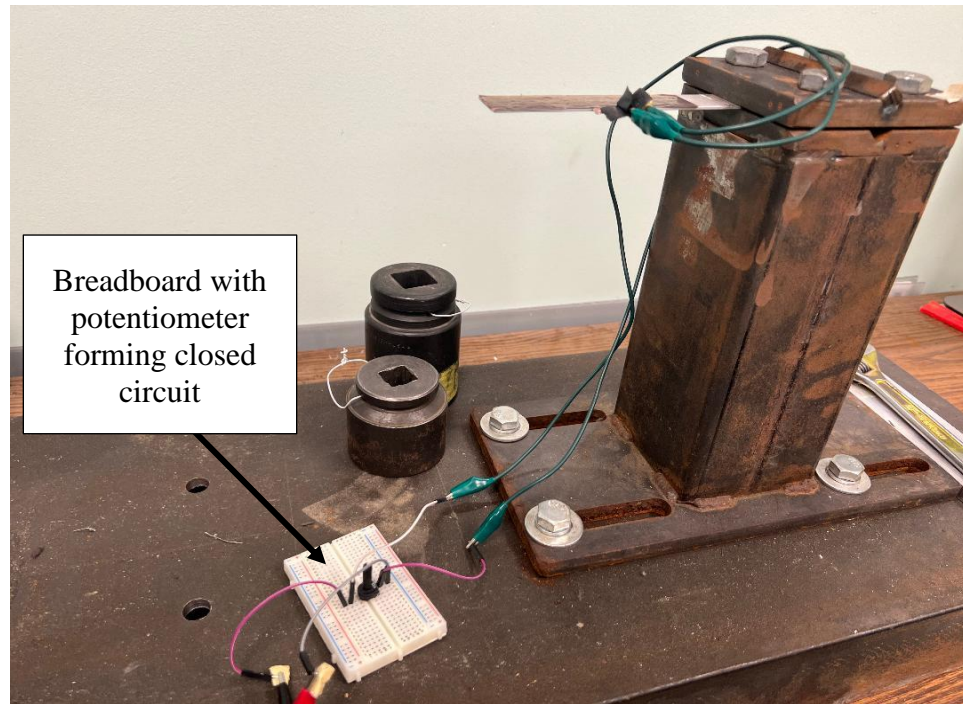
Figure 4-9: Closed circuit with potentiometer to measure voltage drop, current and power.

CHAPTER FIVE

## 5 Results and Summary

5.1 Results

This chapter presents conclusions based on the theoretical development, simulations, and the experimental runs from the preceding chapters of this thesis.

The piezo-mechanical battery was designed to store energy in a spring and release it to be harvested using a PVDF film. The device has a gear ratio of 55:1 and an output speed of 1rev/sec. If the spring has 4 actual turns equaling 4 revolutions of the drive shaft. This gives a runtime of approximately 200secs.

The maximum torque delivered by the spring is 0.08Nm and the dimensions of the escapement mechanism translates the output torque to 0.37N of force on the cantilever beams. This is sufficient to deflect the beam and run the escapement mechanism.

The final assembly of the device is 4 inches tall and 7 inches across and so the objective of portability was somewhat achieved.

The experimental phase was done using weights that equal 12N of force. This produced a deflection of 2.1mm in the aluminum beam substrate. The data recorded by the DAQ system was put through a post-processing code and the results are shown in the figure below.
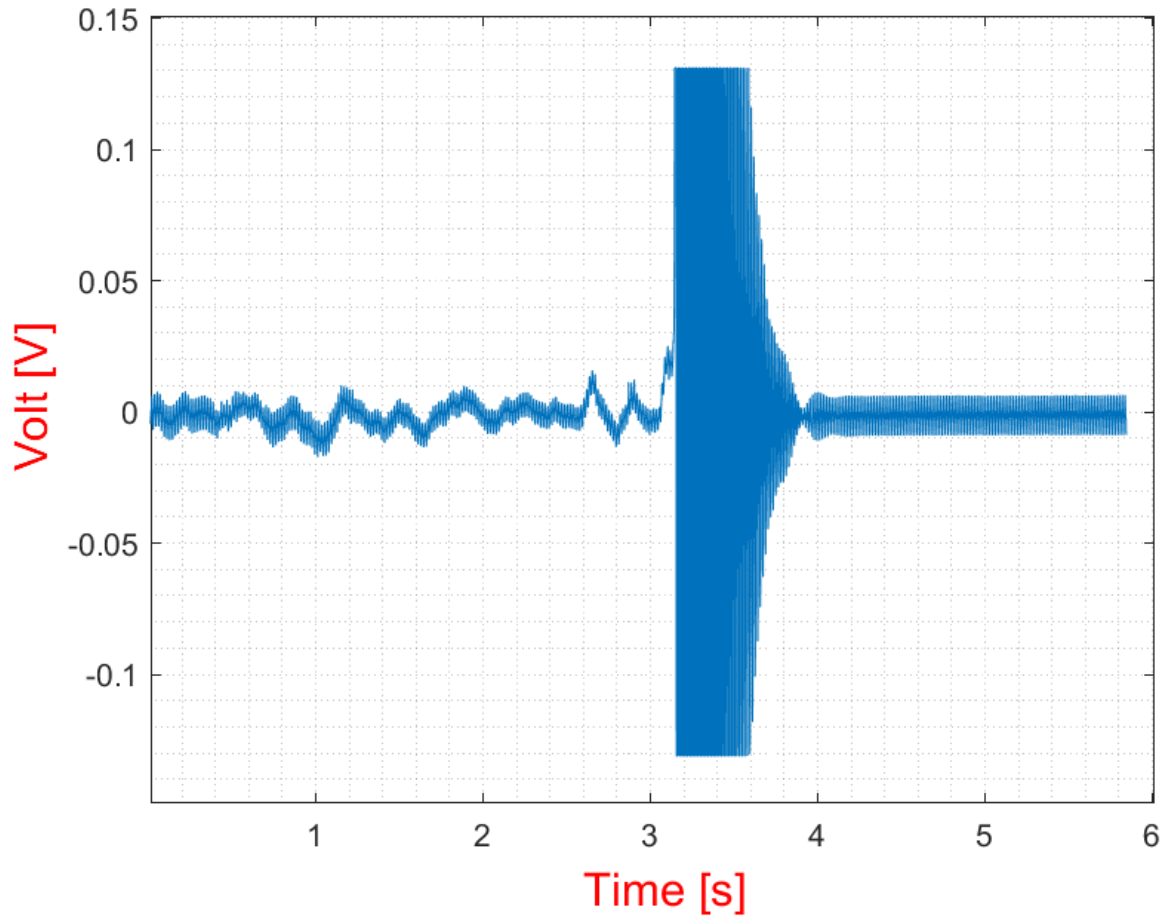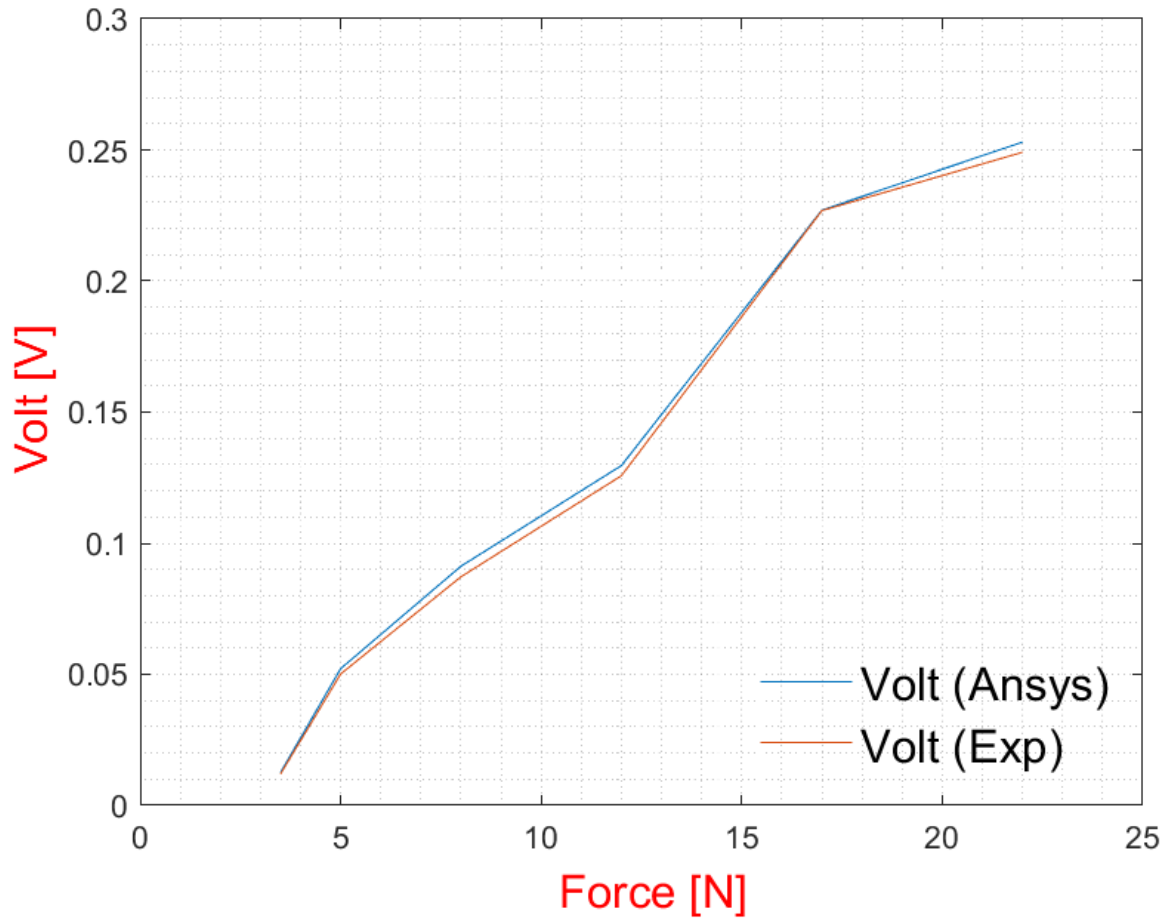
Figure 5-1: Open circuit voltage measured under 12N of force.

The voltage generated and recorded is similar to the voltage seen in the transient structural analysis on ANSYS. There is a 1% error in the results, and this is as a result of imperfect boundary conditions in the experiments.

The peak open-circuit voltage generated was recorded for a range of forces from3.5N to 22N with intervals of approximately 5N. The voltage acquired was compared to the voltage obtained from the FEA of the piezoelectric cantilever beam and the difference calculated as ±3%.

Figure 5-2: Open circuit voltage for a range of forces.

In the second part of the experiment, the circuit was closed, and the voltage measured across a 10kΩ potentiometer. The voltage generated at maximum resistivity was too little to be recorded. The potentiometer was set to the minimum resistance of 6.38Ω and the peak voltage was measured as 0.04V.
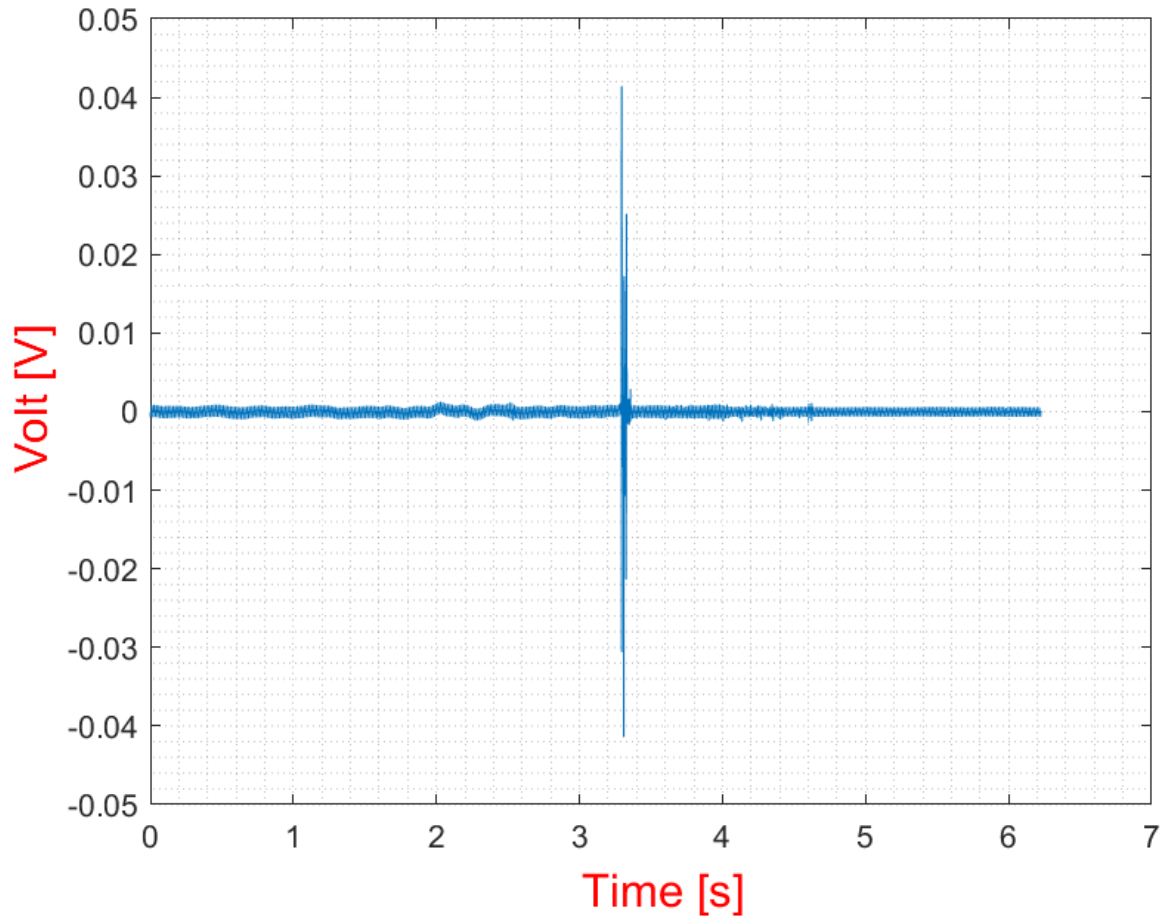
Figure 5-3: Closed circuit voltage measured.

With the value of the voltage and resistance, the current can be calculated from V=IR, as 6.27mA. The power is also calculated as $P=V^2/R$ and this gives a value of 0.251mW.

5.2   Conclusion

In this study, the development of a piezo-mechanical battery was presented, and the results obtained from experiments showed the potential power output of the battery. This shows that the battery concept can be applied to any desired application during the design phase of a machinery by carefully choosing the substrate as well as the boundary conditions of the substrate for the effective function of the sensor.

5.3 Future work

As it stands currently, the battery output is obtained by the post processing of the data collected using code written in MATLAB. While this approach enabled us to show the workability of this battery, the future work will be focused on packaging the battery to include a signal processing electronics to ensure the real-time measurement of voltage.

The concept of the mechanism is proven, and development can be done with stronger materials that can withstand the forces in stronger springs to increase the voltage and power output of the device.

6 APPENDICES

6.1 Appendix A: Labeled section view of the device
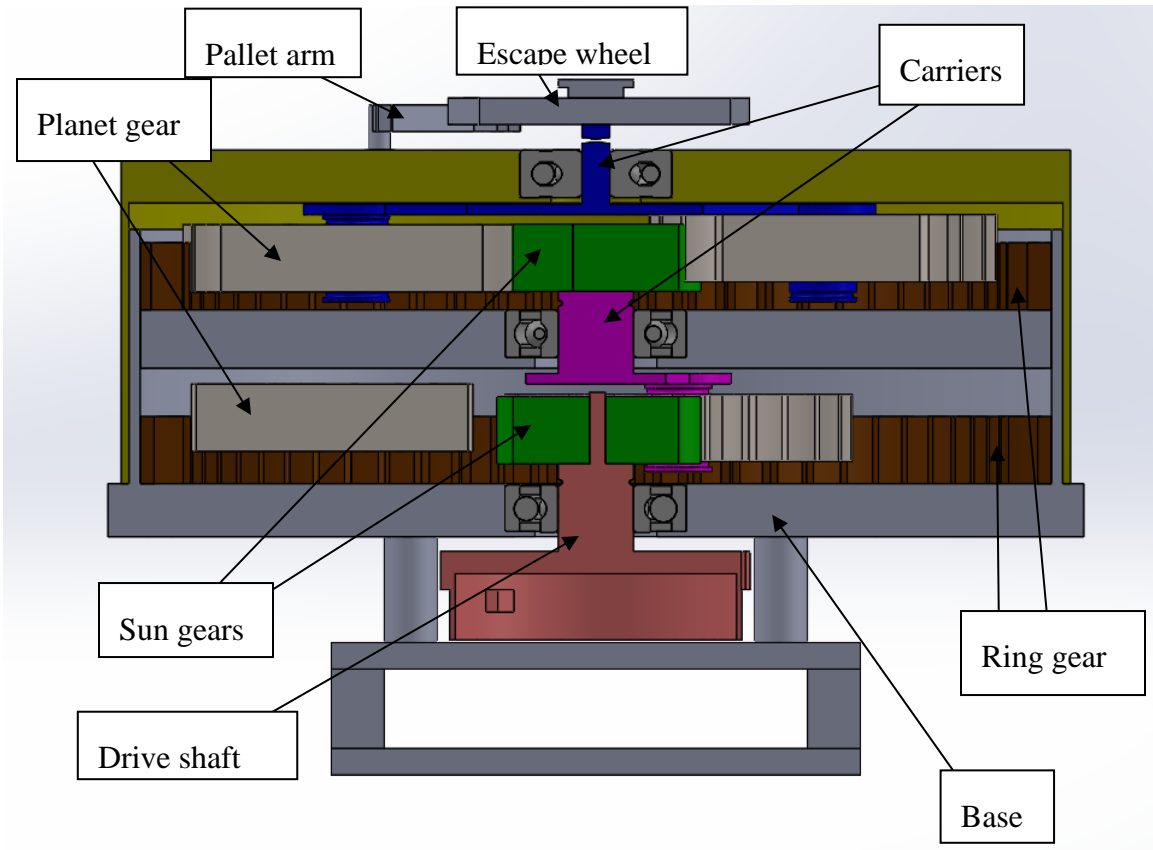
6.2 Appendix B: MATLAB post-processing code

1 Open Circuit Voltage Measurement

```
load 12N1.mat
f=3000; %Hz
t_final=length(LocalDouble)/f;
T=1/f:1/f:t_final;
Volt=LocalDouble;
plot(T,Volt)
grid minor
xlabel('\fontsize{15} \color{red} Time [s]')
ylabel('\fontsize{15} \color{red} Volt [V]')
```

2 Closed Circuit Voltage Measurement across 10K potentiometer

```matlab
load 12NCurrent1.mat
f=3000; %Hz
t_final=length(LocalDouble)/f;
T=1/f:1/f:t_final;
Volt=LocalDouble;
plot(T,Volt)
grid minor
xlabel('\fontsize{15} \color{red} Time [s]')
ylabel('\fontsize{15} \color{red} Volt [V]')
```

REFERENCES

A. Kuoni, e. a. (2003). Polyimide membrane with ZnO piezoelectric thin film pressure transducers as a differential pressure liquid flow sensor. *Journal of Micromechanics and Microengineering*.

al, M. S. (2019). A review of energy harvesting using piezoelectric materials: state-of-the-art a decade later (2008-2018). *Smart Materials and Structures*, 2-3.

Boettcher, D. (2006). *Vintage Watchstraps*. Retrieved from Vintage Watchstraps: http://www.vintagewatchstraps.com/mainsprings.php

Bolaniran, O. A. (2021). *DEVELOPMENT OF A DYNAMIC FORCE SENSOR*. Grand Forks.

BP Statistical review of world energy. (2018, 12 25). Retrieved from BP: https://www.bp.com/content/dam/bp/en/-corporate/pdf/energy-economics/statistical-review/bp-stats-review-2018-full-report.pdf

Bryant, M. W. (2011). Aeroelastic flutter energy harvester design: the sensitivity of the driving instability to system parameters. *Smart Mater. Struct*.

C. D. Richards, M. J. (2004). Efficiency of energy conversion for devices containing a piezoelectric component. *Journal of Micromechanics and Microengineering, vol. 14,*, 717-721.

D., G. (1995). *Piezoelectric generators: material and structures.* Pomiary Automatyka Robotyka.

Energy Storage-Packing Some Power. (2012, March 3). *The Economist*.

Erturk, A. I. (2009). 9 An experimentally validated bimorph cantilever model for piezoelectric energy harvesting from base excitations. *Smart Material Structure*.

Freitas, V. S. (2011). Piezoelectric Characterization of (0.6)BiFeO3–(0.4)PbTiO3 Multiferroic Ceramics. *Journal of the American Ceramic Society*, 754-758.

George, A. J. (2019). *Human Powered Energy Harvester based on Autowinder Mechanism: Analysis, Build and Test.* Clemson Tiger prints.

Goldschmidtboeing, F. a. (2008). Characterization of different beam shapes for piezoelectric energy harvesting. *Micromechanical Microengineering*.

Hill, F. A. (2008). *Energy storage in Carbon Nanotube Super-Springs.* Massachusetts.

Hill, F. A. (2014). Storing energy and powering small systems with mechanical springs made of carbon nanotube yarn. *Energy*.

J. Wu, G. D. (1996). Analogy between the one-dimensional acoustic waveguide and the electrical transmission line for cases with loss. *The Journal of the Acoustical Society of America 100, 3973*.

J.R. Leppe-Nerey, F. S.-E.-P. (2020). Power characteristics of a 70/30 wt.% PVDF/PMMA film in roadway roadwayelectricity generation. *Sensors and Actuators A: Physical*.

Ju, S. &. (2018). Impact-based piezoelectric vibration energy harvester. *Applied Energy, 214,* , 139-151.

Kapelevich, A. (2014). *High Gear Ratio Epicyclic Drives Analysis.* Gear Tachnology.

Kishore, R. A. (2014). Ultra-low wind speed piezoelectric windmill. *Ferroelectrics*.

Kudriavtsev. (1966). *Planetary Gears.* Leningrad: Mashinostroenie.

Li, S. Y. (2011). Ambient wind energy harvesting using cross-flow fluttering . *J. Appl. Phys.*

Myers, R. V. (2007). Small scale windmill. *Appl. Phys*.

Norton, R. L. (2012). *Design of Machinery.* Worcester: McGraw Hill.

Park, J. C. (2013). Asymmetric PZT bimorph cantilever for multi-dimensional ambient vibration harvesting. *Ceram. Int*.

Pradeesh E. L., U. S. (2013). Investigation on various beam geometries for piezoelectric energy harvester with two serially mounted piezoelectric materials. *SN Applied Sciences*.

Prateek Asthana, G. K. (2020). Development of Vibration Piezoelectric Harvesters by the Optimum Design of Cantilever Structures. *Intechopen*.

Priya, S. e. (2005). Piezoelectric windmill: A novel solution to remote sensing. *Japan. J. Appl*.

Q. Wanf, X. D. (1999). Electromechanical coupling and output efficiency of piezolectric bending actuators. *IEEE Transactions on Ultrasonics, Ferroelectrics, and Frequency Control, vol. 46*, 638-646.

Q. Wang, X. D. (1999). Electromechanical coupling and output efficiency of piezolectric bending actuators. *IEEE Transactions on Ultrasonics, Ferroelectrics, and Frequency Control, vol. 46*, 638-646.

R. S. Dahiya, M. V. (2013). *Robotic Tactile Sensing.* Springer.

Roundy, S. e. (2005). Improving power output for vibration-based energy scavengers. *IEEE Pervas. Comput*, 28-36.

S. Roundy, P. K. (2003). A study of low level vibrations as a power source for wireless sensor nodes. *Computer Communications, vol. 26*, 1131-1144.

S. Trolier-McKinstry, S. Z. (2018). High-Performance Piezoelectric Crystals, Ceramics, and Films. *Annu. Rev. Mater. Res*, 191-217.

Safaei, M. (2019). A review of energy harvesting using piezoelectric materials: state-of-the-art a decade later (2008–2018). *Smart Materials and Structures*, 2-3.

Tan, Y. K. (2007). A novel piezoelectric based wind energy harvester for low-power autonomous wind speed sensor . *r IECON 2007 - 33rd Annual Conference of the IEEE Industrial Electronics Society*.

Taylor, G. W. (2001). The energy harvesting eel: a small subsurface ocean/river power generator . *IEEE J. Oceanic Eng.*, 539-547.

Tien, C. M. (2010). Use of a piezo-composite generating element for harvesting wind energy in an urban region. *Aircr. Eng. Aerosp. Technol.*

Wald, M. L. (2010, July 28). Wind Drives Growing Use of Batteries. *The New York Times*, p. B1.

Why Energy Storage-Mechanical Energy Storage. (2022, January 31). Retrieved from Energy storage Association: https://energystorage.org/why-energy-storage/technologies/mechanical-energy-storage/

Wu, N. W. (2015). Ocean wave energy harvesting with a piezoelectric coupled buoy structure. *Appl. Ocean Res.*

Wu, Y. Q. (2018). A piezoelectric spring pendulum oscillator used for multi-directional and ultra-low frequency vibration energy harvesting. . *Applied Energy, 231*, 600-614.

Xie, X. W. (2014). Energy harvesting from transverse ocean waves by a piezoelectric plate. *Int. J. Eng. Sci.*

Yang, Y. e. (2014). 4 Rotational piezoelectric wind energy harvesting using impact-induced resonance. *Appl. Phys. Lett*.